THE PHYSICOCHEMICAL CHARACTERIZATION OF MICROVESICLES SECRETED BY *SULFOLOBUS ACIDOCALDARIUS*

A Dissertation
Submitted to
the Temple University Graduate Board

In Partial Fulfillment
of the Requirements for the Degree
DOCTOR OF PHILOSOPHY

---

by
Alexander P. Bonanno
December 2019

Examining Committee Members:

Dr. Parkson Lee-Gao Chong, Advisory Chair, Biochemistry
Dr. Ana Gamero, Biochemistry
Dr. Dale Haines, Biochemistry
Dr. Brad Rothberg, Biochemistry
Dr. Bettina Buttaro, External Member, Microbiology

ABSTRACT

Microvesicles secreted from the thermoacidophilic archaeon *S. acidocaldarius* (Sa-MVs) contain a membrane made exclusively of tetraether lipids and covered by crystalline surface layer proteins known as the S-layer. While tetraether lipids and S-layer proteins are known to be useful biomaterials, little has been done to exploit Sa-MVs for any scientific applications. In the present study, as the start point to explore this area, we isolated Sa-MVs and used dynamic light scattering, laser Doppler electrophoresis, and cryo-transmission electron microscopy (cryo-TEM) to characterize the particle size, size distribution, zeta potential, and morphology of Sa-MVs and tested their stabilities against temperature, pH, autoclaving, and the detergent Triton X-100. We found that, at the cell's growth pH (~2.6) and growth temperature (75-80^{o}C), Sa-MVs in the growth medium are ~180-183 nm in diameter with a polydispersity index (PDI) $\leq$ 0.15 and have a zeta potential of -0.5 mV. Sa-MVs in buffer exhibited long-term (at least 137 days) stability with no signs of vesicle disintegration or fusion. When the pH was decreased from 7.2 to 2.6, the average size of Sa-MVs was increased by ~40-45 nm, which probably came from conformational changes of S-layer proteins, in concomitant with vesicle aggregation, but not due to conformational changes in tetraether lipid headgroups. The isoelectric point (pI) for Sa-MVs in 1 mM KCl is 3.0 while that for the reconstituted liposomes (LUV_{MV}) is estimated to be below 2.0. Sa-MVs dispersed in buffer at pH 2.6 change little in size over five autoclaving cycles, despite becoming slightly less spherical after autoclaving, while at this pH liposomes made of diester lipids cannot sustain multiple cycles of autoclaving. In addition, compared to diester and PLFE liposomes, Sa-MVs and LUV_{MV} exhibit unusual

resistance against the surfactant Triton X-100. Although some man-made liposomes such as PLFE liposomes are also stable against temperature, pH, and other environmental stressors, Sa-MVs are unique in that they are naturally occurring nanoparticles with a native membrane environment suitable for inserting additional lipids and membrane-bound proteins as needed. With their great stability presented here and the lack of cytotoxicity known in the literature, Sa-MVs hold great promise for technological applications.

In addition to these biophysical techniques employed to characterize these microvesicles, a series of fluorescence experiments have also been conducted to gain further insight into how the membrane packing of these vesicles compares to tetraether as well as diester liposomes. Intrinsic protein fluorescence of native microvesicles was examined to characterize the dynamics of the *S. acidocaldarius* MVs. We have used the probe 6-lauroyl-2-dimethylaminonaphthalene (Laurdan) to monitor membrane packing and dynamics within the water-membrane interfacial region of the Sa-MVs. Specifically, we measured Laurdan's generalized polarization (GP), which depends on the probe's local polarity, probe location and nearby viscosity. We also measured Laurdan's red edge excitation shift (REES), which depends on the dynamics of solvent relaxation around the fluorophore compared to the probe's fluorescence lifetime. As temperature increased from 18 to 66.7 °C, GP decreased from 0.026 to –0.118. Comparing the GP values of reconstituted vesicles to that of the native Sa-MVs, it appears that the two curves are similar in both GP value and trend over increasing temperature range (values decrease from 0.112 to -0.215), which suggests that Laurdan in Sa-MVs resides in the lipid membrane, not in proteins and that Laurdan's GP is not affected much by the presence of Sa-MV proteins. It is well known that, for liposomes made of diester lipids, the GP value of Laurdan

fluorescence is high in the gel state and low in the liquid-crystalline state, with an abrupt change during the phase transition. However, Laurdan's GP values obtained from liposomes comprised of tetraether lipids such as PLFE and Sa-MV lipids cannot be compared directly to those obtained from diester liposomes and cannot be interpreted simply based on membrane packing because probe location and chromophore orientation in tetraether liposomes could be distinctly different from those in diester liposomes. Our data show that the REES effect in PLFE LUVs is most pronounced among all the membranes examined showing a value of 10.58 nm at 24^{o}C compared to 0.9 nm for DMPC LUVs at the same temperature. It is already known that membrane packing in PLFE liposomes is extraordinarily tight partly due to the strong hydrogen bond network in the polar head group regions where the phosphate and sugar moieties are abundant and partly due to the rigid and ordered dibiphytanyl hydrocarbon chains. Since the chromophore of Laurdan in PLFE liposomes is most likely located in the membrane-water interfacial region, it is not surprising that solvent tumbling around Laurdan in PLFE LUVs is much more restricted in PLFE LUVs than in DMPC LUVs, giving rise to a much higher REES value in PLFE LUVs than in DMPC LUVs.

The REES values (10.3-14.1 nm) of Laurdan fluorescence in LUVs reconstituted from the extracted MV lipids are higher than those (9.3-10.6 nm) in PLFE LUVs, which suggests that the mobility of solvent molecules (including water and lipid polar groups) in the membrane-water interfacial regions of LUV_{MV} is much less restricted than that in PLFE LUVs. Like PLFE, Sa-MV lipids are tetraethers. However, as mentioned earlier, PLFE lipids are different from Sa-MV lipids in their hydrophobic core composition. It is likely that their polar head groups are also different despite that the zeta potentials of LUV_{PLFE}

and LUV_{MV} are virtually identical (−43 mV in 50 mM Tris buffer containing 10mM EDTA and 0.02% NaN_3 at pH 7.2-7.6 and 25°C).

The REES values (14.5-18.9 nm) of Laurdan fluorescence in Sa-MVs are higher still than those of both LUV_{PLFE} and LUV_{MV}, which is reasonable because tetraether lipids in Sa-MVs are covered with S-layer proteins. As a result, the mobility of solvent molecules around Laurdan's chromophore in the lipid polar head group regions is more restricted than that in LUV_{PLFE} or LUV_{MV}.

Free-standing planar membrane made of MV lipids built on a cellulose acetate partition and mounted onto a Teflon device sustained a nearly constant capacitance (~36-39 pF) for 8 h. Thereafter, the membrane collapsed as evidenced by a zero capacitance. In contrast, the planar membrane made of the diester lipid POPC had much lower stability, showing large fluctuations in capacitance before its collapse at 1.5 h, a very short lifetime typical for free-standing planar membranes made of diester lipids. The planar membrane made of the diester lipid DMPC also showed a short lifetime ~3h. In comparison, the planar membrane made of PLFE showed remarkable stability, exhibiting a constant capacitance for at least 11 days. Similar high stability of PLFE free-standing planar membranes over micro-pores on PDMS thin films in microchip platform was previously reported.

Our data suggest that lipids extracted from *S. acidocaldarius* MVs are able to form fairly stable free-standing planar membranes across a pinhole on a solid support. However, even though both MV lipids and PLFE lipids are tetraethers, the planar membrane made of MV lipids is not as stable as that made of PLFE lipids. The molecular basis for the differential stability between planar membranes of MV lipids and PLFE lipids is not clearly understood at present, but the difference in stability is likely to originate from the chemical

structure differences between PLFE lipids and MV lipids. As mentioned earlier, in terms of the hydrophobic cores, PLFE contains ~90% GDNT and ~10% GDGT, whereas MV lipids are mainly GDGT and GTGT, without any GDNT, and their headgroup structures are not known. We have also demonstrated the ability to observe channel activity in PLFE monolayers at a range of voltages from -200 to 200 mV. However, this was property was not replicated in lipids extracted from *S. acidocaldarius* microvesicles. In any case, our past and present data showed that archaeal tetraether lipids are excellent materials to make stable and yet biologically relevant free-standing planar membranes.

This dissertation is dedicated to the friends I've made at Temple.

"If it can't be autoclaved, I don't want to eat it"

TABLE OF CONTENTS

Page

ABSTRACT iii

DEDICATION viii

LIST OF TABLES xi

LIST OF FIGURES xii

LIST OF ABBREVIATIONS xiv

CHAPTER

1. INTRODUCTION 1

    1.1 *Sulfolobus acidocaldarius* 1

    1.2 Archael Bipolar Tetraether Lipids 2

    1.3 Microvesicles 4

    1.4 Planar Membranes and Protein Incorporation 9

2. STATEMENT OF GOALS 13

    2.1 Aim 1 13

    2.2 Aim 2 14

    2.3 Aim 3 15

3. METHODS 16

4. RESULTS PART 1 25

    4.1 Long-term stability of Sa-MVs 25

    4.2 Sa-MV stability against temperature and pH 27

4.3 Sa-MV stability against autoclaving 38

4.4 Sa-MV stability against the detergent Triton X-100 41

5. RESULTS PART 2 45

5.1 Intrinsic protein fluorescence 45

5.2 Laurdan fluorescence 60

6. RESULTS PART 3 73

6.1 Free standing planar membranes 73

6.2 Functional protein incorporation 76

7. DISCUSSION 81

BIBLIOGRAPHY 87

LIST OF TABLES

Table Page

1. **Steps involved in the isolation of Sa-MVs from the *S. acidocaldarius* cell suspensions**……..……..... 18

2. **Sa-MV size and poly dispersity index** ……..…..….... 48

3. **Effect of temperature on the emission maximum of Sa-MV** ……..…….... 58

4. **Sa-MV REES values.** ……..…..... 72

LIST OF FIGURES

Figure Page

1. **Illustration of the hydrophobic core structures of tetraether lipids found in the plasma membrane (GDNT, GDGT, and GTGT) and microvesicles (GDGT and GTGT) of the *Sulfolobus thermoacidophiles*** ……. 7

2. **Long term stability of Sa-MVs** ……..…..…… 26

3. **Temperature dependence of the average particle size, PDI, and zeta potential of Sa-MVs** ……..…… 29

4. **Effects of pH on the particle size and PDI of Sa-MVs in 1 mM KCl at room temperature** …… 32

5. **Effects of pH on the particle size and PDI of LUV$_{MV}$**……..……. 33

6. **Effects of pH on the zeta potential of Sa-MVs and LUV$_{MV}$**…… 36

7. **Negative staining cryo-TEM images of Sa-MVs and LUV$_{MV}$**…… 37

8. **Stability of Sa-MV and various LUVs against autoclaving**…… 40

9. **Stability of Sa-MVs and various unilamellar vesicles (LUVs) of lipids against the surfactant Triton X- 100**……... 42

10. **Effect of dialysis on the technical emission spectra of Sa-MVs isolated from *S. acidocaldarius* cell suspensions**…… 46

11. **The effect of TDM on the particle size and absorption spectrum of Sa-MVs**.....…… 53

12. **Absorption spectra of undialyzed Sa-MVs**..... 55

13. **Effect of temperature on the intrinsic protein fluorescence of dialyzed Sa-MVs**…….. 59

14. **Effects of temperature on Laurdan's excitation generalized polarization (GP) in Sa-MVs and in various liposomes as indicated**…… 63

15. **Illustration of technical emission spectra of Laurdan fluorescence in Sa-MVs and various liposomes**……. 67

16. **Effect of temperature on REES in Sa-MVs and various liposomes**…….. 71

17. **Stability of various free standing planar membranes**……. 75

18. **MTHK channel activity in PLFE or MV lipid**…… 78

19. **5,(6)CF intensity change as reflected by pH decrease within liposomes**… 81

20. **Graphical summary**..... 86

LIST OF ABBREVIATIONS

BTL	bipolar tetraether lipid
CMC	critical micelle concentration
Cryo-TEM/TEM	cryo transmission electron microscopy
DMPC	1,2-dimyristoyl-sn-glycero-3-phosphocholine
DPPC	dipalmitoyl-L-α-phosphatidylcholine
EV	Extracellular vesicle
GDGT	glycerol dialkyglycerol tetraether
GDNT	glycerol dialkylcalditol tetraether
GP	generalized polarization
GTGT	trialkyl glycerol tetraether
GUV	giant unilamellar vesicle
LUV	large unilamellar vesicle
MTHK	calcium-gated potassium channel from *Methanobacterim thermoautotrophicum*
MV	microvesicle
PDI	polidispersity index
PDMS	polydimthylsiloxane
PLFE	polar lipid fraction E
POPC	1-palmitoyl-2-oleoyl-sn-glycero-3-phosphocholine
REES	red-edge excitation shift
Sa-MV	*Sulfolobus acidocaldarius* microvesicles
TDM	n-tetradecyl-β-D-maltoside
ZP	zeta potential
$\lambda_{em,max}$	Emission maximum
C_r	Critical concentration

CHAPTER # 1

INTRODUCTION

1.1 *Sulfolobus acidocaldarius*

The kindom archaea is divided into two sub groups: euryarchaeota and crenarchaeota (1). The group crenarchaeota contain groups of thermophilic archaea, whereas euryarchaeota include halophiles and methanogens. *Sulfolobus acidocaldarius* are a thermoacidophilic species of archaea that were first discovered to exist living in the hot springs in Yellowstone National Park. Optimal growth conditions were determined to be at pH between 2 and 3 and a temperature between 75 and 80 degrees Celsius. Primarily, the organism grows aquatically, but they have also been found in hot acidic soil. The organism can grow both heterotrophically and autotrophically on sulfur or other naturally occurring compounds, oxidizing sulfur crystals to sulfuric acid. *S. acidocaldarius* are responsible for the sulfuric acid conditions in their aquatic environment (2). They have been described as having a lobed sphere shape, and a cell wall that is completely lacking in peptidoglycan. Notably, the lipid composition comprising the cell membrane is made of about 95% tetraether lipids, which is thought to be how the organism can survive such harsh conditions. (3) (4).

1.2 Archaeal Bipolar Tetraether Lipids

Due to the harsh conditions in which archaea live, their cell membranes have adapted highly specialized traits that enable them to survive. They have adapted to produce Bipolar tetraether lipids (BTLs), which are present in all three major archaeal phylums: euryarchaeota, crenarchaeota and thaumarchaeota. The group euryarchaeota include methanogens and halophiles. BTLs are present in methanogens (0–50%), but virtually absent in halophiles. BTLs are also found in thaumarchaea, which grow in much more ambient conditions. BTLs are the dominating lipid species in crenarchaeota (~90–95% of the total lipid extract), which thrive under high temperature and low pH conditions (5).

The lipids synthesized by these extremophiles, namely, *S. acidocaldarius*, consist mostly of a mixture of glycerol dialkylcalditol tetraether (GDNT) and glycerol dialkyglycerol tetraether (GDGT), both members of a class of BTLs (6-8). BTLs are the dominating lipid species in *S. acidocaldarius*, comprising up to 95% of the total lipid makeup (9). The structures of these lipids are all either macrocyclic or hemi-macrocyclic. In *S. acidocaldarius,* the hydrophobic core region of macrocyclic BTLs contain two biphytanyl (ie 20 carbon long) chains. These chains are both saturated, containing varying numbers of cyclopentane rings and branched methyl groups. The amount of cyclopentane rings present in each of the dibiphytanyl chains can increase (up to 8 per molecule) with increasing temperature growth (10). These rings limit the gauchian space in the hydrophobic core of the lipids and thereby increase packing tightness, lending to increased stability in harsh conditions. The chains are connected to either glycerol or calditol backbones, lending to their cyclical shape (11).

Also present in *Sulfolobus acidocaldarius*, albeit to a much smaller degree, are hemi-macrocyclic lipids. These lipids are characterized by one biphytanyl chain with both ends linked to a different glycerol moiety, and two phytanyl chains, each linked to a glycerol backbone (12).

The polar lipid fraction E (PLFE) extracted from *Sulfolobus acidocaldarius* contains a mixture of GDNT and GDGT. The GDNT component (~90% of total PLFE) contains phospho-*myo*-inositol on the glycerol end and β-glucose on the calditol end, whereas the GDGT component (~10% of total PLFE) has phospho-*myo*-inositol attached to one glycerol and β-D-galactosyl-D-glucose to the other glycerol skeleton. The hydrophobic region of PLFE contains a pair of 40-carbon biphytanyl chains with isoprene units. Each biphytanyl chain includes up to four cyclopentane rings. PLFE lipids have incredible stability against high temperature, pressure, low pH, and auto-oxidation, fusogenic compounds, and lipases (13,14). Also, PLFE lipids containing liposomes are not toxic which makes PLFE lipids suitable for biological research (15). These characteristics demonstrate the usefulness of PLFE lipids especially in liposomal formulation. Examples of these lipids can be seen in Figure 1.

1.3 Microvesicles

Microvesicles (MVs), along with exosomes, ectosomes, and other small particles, are a type of cellular vesicle under the larger umbrella term extracellular vesicles (EVs) (16). These types of vesicles differ in size, origin, and function. Exosome is a term reserved for particles between 40 and 100 nm in size, that result from the fusion of multivesicular bodies to the plasma membrane, causing vesicle release (16). MVs, however, are a term used for vesicles typically of a larger size, that originate from budding off of the plasma membrane. MVs are released by numerous cell types in every phylogenetic kingdom including archaea (17,18). Originally, the physiological role of MVs was dismissed as, they were referred to as "cell waste" or "cell dust" (19). However, at present, the biochemical and physiological role of mammalian and prokaryotic MVs have been extensively characterized. EVs from various sources were found to contain mRNA, miRNA, which can be translated into proteins by recipient cells (20). EVs were also found to contain a number of proteins, lipids, carbohydrates, and DNA, as they contain cytoplasmic contents of the cells from which they are derived (21,22). Being that most of this type of work has been done in eukaryotic and bacterial EVs, the role of MVs in archaea is a budding area of research.

There is a stark difference in biochemical composition between MVs released from the thermoacidophlic archaeon *Sulfolobus acidocaldarius* (optimum growth: 75-80^{o}C and pH 2-3) and those found in the bacterial and animal kingdoms (23). MVs released from bacteria and animal cells contain hundreds of distinct proteins (24,25) whereas MVs released from *S. acidocaldarius* (Sa-MVs) have only 29 unique proteins according to the

work of Ellen et al. (23). The simplicity in protein composition makes Sa-MVs an attractive model system for studying the mechanism of MV formation (23). Due to the presence of certain specific proteins, it has been speculated that MVs released from the archaea phylum *Sulfolobus* play a role in transferring DNA from cells to cells at high temperatures (26), transporting toxic compounds such as sulfolobicins into the surrounding milieu (18), transferring thiosulfate to sulfur receptors to protect the electron transport chain from inhibition by hydrogen cyanide or hydrogen sulfide (23), and cell adhesion or biofilm formation (23). However, much more basic research is needed in order to fully unravel the biological functions of Sa-MVs.

The most abundant protein species in Sa-MVs are the S-layer proteins, which cover the surface of the microvesicles and presumably originate from the S-layer proteins on the cell membranes (23). In fact, all *Sulfolobales* have two S-layer proteins, namely, SlaA and SlaB (27). They self-assemble to form a regular array of pores with a p3 symmetry (28). The S-layer is tough but porous, and permeable to small molecules through the pores (2-8 nm) (29). Because of their protective role and their capability to self-assemble and serve as molecule and ion traps, the S-layer proteins from bacteria and archaea have found a variety of biotechnology applications such as biocatalysis, vaccine development, drug delivery, and biochip development (30). Conceivably, Sa-MVs, with their surfaces also covered by S-layer proteins, may be developed into useful biomaterials as well.

Sa-MVs also have unusual lipid compositions. First, the lipids of Sa-MVs are exclusively tetraethers whereas most of the lipids in mammalian or bacteria MVs are diesters. Tetraether and diester lipid membranes have distinct physicochemical properties

(31). Membranes made of tetraether lipids such as the polar lipid fraction E (PLFE) isolated from *S. acidocaldarius* are much more tightly packed and more stable than membranes made of diester lipids (3,32). Because of this remarkable membrane property, nano-scale liposomes made of archaeal or synthetic tetraether lipids (termed as archaeosomes) have been exploited as drug or gene carriers with extraordinary stability (33-39). It is possible that the tough tetraether lipid membrane plus the outermost and strong S-layer would make Sa-MVs particularly appealing as naturally occurring nanomedicine. However, little has been explored on this subject.

Second, Sa-MVs have glycerol dialky glycerol tetraether (GDGT or caldarchaeol; Figure 1) as the dominating lipid hydrophobic core structure (99.8% by weight, calculated from Table 1 of (23)), glycerol trialkyl glycerol tetraether lipid (GTGT, Figure 1) as a very minor lipid component (0.2% by weight, calculated from Table 1 of (23)), and no glycerol dialky calditol tetraether (GDNT or calditolglycerocaldarchaeol; Figure 1) (23). This finding is surprising because Sa-MVs are supposed to derive from the cell's plasma membrane where GDNT is the major lipid component (~70% (w/w) of the total isoprenoid ethers) while GDGT comprises a smaller fraction (~20% (w/w)) (12). This finding makes Sa-MVs an attractive model system for studying the mechanism of MV formation (23).

Since Sa-MVs have interesting protein and lipid compositions and since membrane compositions are tightly associated with membrane properties (40), it is of interest to characterize the physical properties of Sa-MVs as the start point to interrogate the biological role of Sa-MVs and to develop Sa-MVs for technological applications.

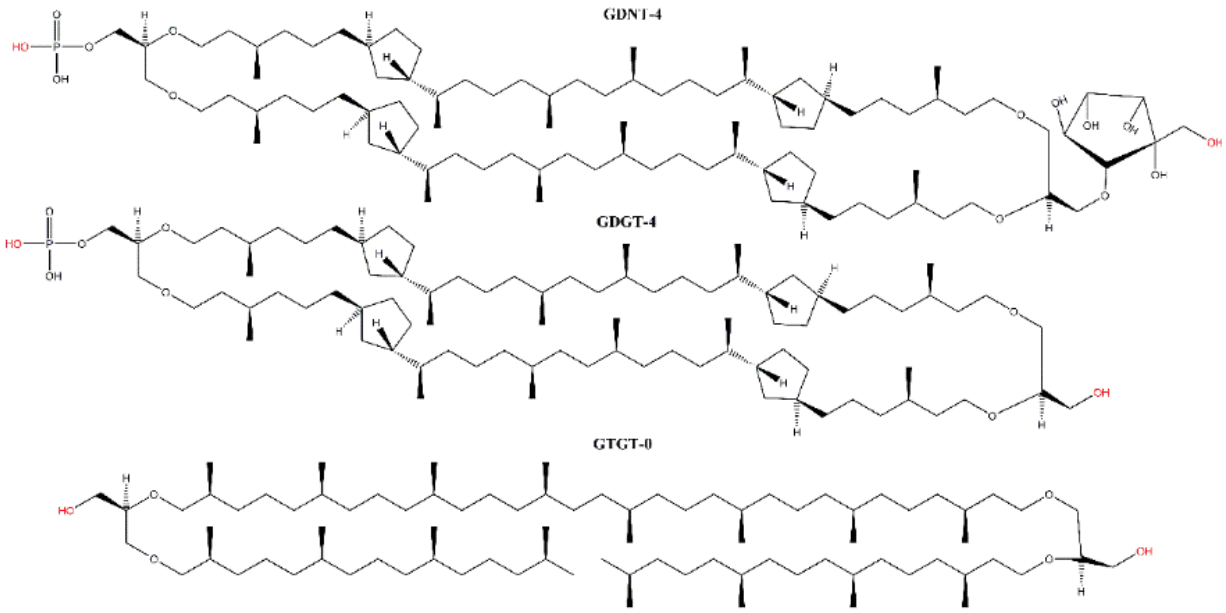

Figure 1. **Illustration of the hydrophobic core structures of tetraether lipids found in the plasma membrane (GDNT, GDGT, and GTGT) and microvesicles (GDGT and GTGT) of the *Sulfolobus thermoacidophiles***. The number after the abbreviations indicates the number of cyclopentane rings per molecule. In the cases of GDNT and GDGT isolated from *S. acidocaldarius*, this number can vary from 0-8.

In the present study, we have isolated MVs from *S. acidocaldarius* (Sa-MVs) and used dynamic light scattering, laser Doppler electrophoresis, and cryo-transmission electron microscopy (cryo-TEM) to characterize the particle size, size distribution, zeta potential, and morphology of Sa-MVs and tested their stabilities against temperature, pH, autoclaving, and the surfactant Triton X-100. We have also dissected the physical properties to see if they are derived from lipids or proteins by studying liposomes made of lipids extracted from Sa-MVs. The results obtained from liposomes reconstituted from Sa-MV lipids (thus protein free) are compared with those obtained from liposomes made of the polar lipid fraction E (PLFE) lipids isolated from *S. acidocaldarius*. PLFE is one of the major polar lipid fractions purified from the plasma membrane of *S. acidocaldarius*. PLFE contains ~90% GDNT and ~10% GDGT (8). Liposomes and planar membranes made of PLFE lipids have been shown to exhibit remarkable stability and unusually tight membrane packing properties (32,41). Since Sa-MVs are made up of GDGT and GTGT whereas PLFE liposomes are composed of GDNT and GDGT, significant differences in physical properties between PLFE liposomes and the liposomes reconstituted from Sa-MV lipids are expected, which may help reveal the structure-activity relationship in archaeal membrane systems.

Additionally, we used fluorescence spectroscopy, in conjunction with dynamic light scattering, absorption spectroscopy, and surfactant treatment, to further characterize the physical properties of Sa-MVs. We employed both the Sa-MV's intrinsic protein fluorescence and the fluorescence from the extrinsic membrane probe 6-dodecanoyl-2-dimethylaminonaphthalene (Laurdan). Specifically, we used the emission and

excitation/absorption spectra of Sa-MV proteins to assess the environment near the tryptophan and tyrosine residues and test if there exist H- or J-aggregates of protein chromophores. We also used the generalized polarization (GP) and the red edge excitation shift (REES) of Laurdan fluorescence to examine the solvent relaxation and motional restriction of the probe in Sa-MV membranes. The GP and REES values of Laurdan fluorescence in Sa-MVs are compared with those obtained from the unilamellar vesicles (LUVs) made of the polar lipid fraction E (PLFE) lipids isolated from *S. acidocaldarius* (LUV_{PLFE}) and the LUVs reconstituted from the tetraether lipids extracted from Sa-MVs (LUV_{MV}) as well as the LUVs made of the synthetic diester lipids. PLFE is composed exclusively of tetraether lipids GDNT (~90%) and GDGT (~10%) (8), whereas Sa-MV lipids are made of GDGT and GTGT. Our data allows us to evaluate whether this lipid compositional difference leads to differential membrane behaviors among Sa-MVs, LUV_{PLFE}, and LUV_{MV}. The results obtained from this study shed light on the dynamic structures of Sa-MVs and pave the way for future studies on the structure-activity relationship of Sa-MVs and the development of Sa-MVs as naturally occurring nanoparticles for technological applications (42).

1.4 Planar Membranes and Protein Incorporation

The use of free standing planar membranes has been an important tool for studying protein channels, lipid stability, and ion flux for decades. In recent years, microfluidic devices are in development to aid in processes such as drug screening (43), pathogen detection (44), artificial photosynthesis (45), and biophysical studies of ion channels (46). These membranes are appealing as biophysical tools because access to both sides of the

membrane is ideal for buffer exchange and measurements such as single ion channel conductance (46).

A major obstacle to using diester lipid membranes on a solid support is their stability. Studies have shown that these membranes fail, causing loss of membrane capacitance, in just 2-4 hours (47). Efforts to improve this stability have proven unsuccessful, expensive, and yielding results with questionable physiological or biological significance with the use of artificial systems. For example, shrinking pore size has been an approach previously taken, but expensive facilities and lack of material availability are more troublesome obstacles to overcome (48). Also, artificial materials such as polydimethylsioxane (PDMS) or triblock copolymers have been used to generate stable membranes, but the lack of physiological relevance and dramatic difference of physical properties between these artificial membranes and mammalian or bacterial cellular membranes brings the results of these studies into question (49).

Archaeal BTLs, such as PLFE, have been shown to form stable free standing planar membranes (50). The characteristic features of BTLs that lend to increased stability in both cellular and liposomal membranes lend drastically different properties to planar membranes derived from diester lipids. For example, BTL planar membranes usually form a monomeric membrane, with individual lipid moieties oriented upright, as opposed to a bilayer (51).

Lipid dynamic simulations have shown that the ether linkages and branched chain methyl groups in BTLs, as opposed to the ester linkages and lack of branched chains in diester lipids, contribute significantly to lipid tangling amongst adjacent lipid molecules

(52). This tangling significantly reduces motion within the membrane, therby lending to greater stability (53). Additionally, more tightly packed lipid membranes reduce lipid motion speed, which restricts the permeability of most small molecules, such as water, which can create hydrophilic pores causing membrane collapse (54). However, the potential of this field is vast, and more basic work characterizing the physical properties of these lipids needs to be done to assess whether archaeal BTLs could provide a stable and biologically relevant solution to these issues. In this section, the stability of free standing PLFE membranes will be directly compared to diester lipid membranes, as well as tetraether lipids extracted from Sa-MVs.

In order to demonstrate potential applications in the biotechnological world, we have looked at the potential functionality of two proteins in tetraether lipid based systems. First, MTHK was isolated from the crenarchaeon *Methanothermobacter thermautotrophicus*. MTHK is an inwardly rectifying, calcium gated potassium channel (55). This channel is used as a model for calcium dependent potassium channels in the field. This channel was chosen because the archaea from which it was isolated is also thermophilic, growing at 65 ˚C and containing tetraether lipids (56).

We also examined bacteriorhodopsin in liposomes made of tetraether lipids, for the purpose of establishing the initial foundation for artificial photosynthesis. Upon exposure to light, BR reconstituted in tetraether liposomes in conjunction with another protein, FoF1-ATP synthase, will generate a proton gradient. This will lead to ATP production from ADP via the synthase protein. (57,58). This work has been conducted before using diester

lipids, and the instability of the vesicles are a potential pitfall of these experiments. Using a highly stable tetraether lipid system would remedy this.

CHAPTER # 2

STATEMENT OF GOALS

PART 1: *Sulfolobus acidocaldarius* microvesicles are naturally occurring nanoparticles with unusual stability against various environmental stressors

In this section, as the start point to exploit Sa- MVs for biotechnology applications, we used dynamic light scattering, laser Doppler electrophoresis, and cryo- transmission electron microscopy to characterize Sa-MVs and tested their stabilities against various environmental stressors and compare their stability to unilamellar vesicles composed of both diester lipids and other tetraether lipids. **We hypothesize that Sa-MV have similar resistance to environemental stressors as PLFE liposomes, much greater than conventional diester liposomes.**

I. Assess the long term stability of Sa-MVs using dynamic light scattering (DLS)

II. Determine Sa-MV stability against temperature and pH

   a. Monitor both Sa-MV and LUV_{MV} size and poly dispersity from room temperature (~25 ˚C) to native growth temperature (75-80 ˚C) in native growth media and buffer system

   b. Monitor both Sa-MV and LUV_{MV} size and poly dispersity over a wide pH range (native growth pH 2.6 – near-neutral pH 7.2)

   c. Using Cryo-EM, image both Sa-MV and LUV_{MV} at different pHs

III. Determine Sa-MV and LUV_{MV} stability against autoclaving

IV. Comparison of Sa-MV and various unilamellar vesicle stability against the detergent Triton X-100

PART 2: *Sulfolobus acidocaldarius* Microvesicles Exhibit Unusually Tight Packing Properties as Revealed by Optical Spectroscopy

In this section, we used optical spectroscopy to characterize the physical properties of microvesicles released from the thermoacidophilic archaeon *Sulfolobus acidocaldarius* (Sa-MVs) by exciting the intrinsic tryptophan and tyrosine residues associated with the proteins on Sa-MV, and by use of the extrinsic probe 6-dodecanoyl-2-dimethylaminonaphthalene (Laurdan). **We hypothesize that membrane packing tightness in Sa-MV and LUVMV is similar to or greater than that seen in PLFE liposomes.**

I. Intrinsic protein fluorescence
    a. Effect of dialysis on technical emission spectra
    b. Effect of the detergent TDM on particle size and absorption spectra of Sa-MV
    c. Effect of dialysis on absorption spectra
    d. Effect of temperature on intrinsic protein fluorescence

II. Laurdan fluorescence
    a. Comparison of Laurdan generalized polarization (GP) in tetraether lipid vesicles and diester lipid vesicles
    b. Comparison of Laurdan red edge excitation shift (REES) in tetraether lipid vesicles and diester lipid vesicles

PART 3: Planar membranes and protein incorporation into tetraether lipid membranes

In this section, we assess the stability of tetraether lipid systems to form free standing planar lipid membranes for possible applications in biotechnology and artificial photosynthesis. We also look to assess the the functionality of these membranes by incorporating and observing functional protein. **We hypothesize that tetraether lipids will form much more stable planar membranes than conventional diester lipids, and are capable of incorporating functional protein.**

I. Demonstrate the ability of PLFE and MV lipid to form stable free standing membranes with stable capacitance
II. Demonstrate insertion of functional MTHK channel in free standing tetraether lipid membranes
III. Demonstrate functional insertion of Bacteriorhodopsin in PLFE liposomes

CHAPTER # 3

MATERIALS AND METHODS

3.1 Materials

1-Palmitoyl-2-oleoyl-*sn*-glycero-3-phosphocholine (POPC), 1,2-dipalmitoyl-*sn*-glycero-3-phosphocholine (DPPC), and 1,2-dimyristoyl-sn-glycero-3-phosphocholine (DMPC) were purchased from Avanti Polar Lipids (Alabaster, AL). 6-Lauroyl-1,2-dimethylamino naphthalene (Laurdan) was purchased from Molecular Probes (Eugene, OR)

3.2 Growth of archaea and isolation of PLFE lipids

S. acidocaldarius cells (strain DSM639; ATCC) were grown aerobically and heterotrophically at ∼75 ˚C, pH ∼2.6. The growth medium contained 0.005% yeast extract, 0.098% trypton, 9.63 mM KH_2PO_4 , 5.43 mM glucose, 0.12 mM $CaCl_2 \cdot 2\ H_2O$, 0.52 mM MgSO 4 • 7 H_2O, 19.07 μM Fe(NH_4) citrate, 2.77 μM $MnCl_2 \cdot 4\ H_2O$, 5.66 μM H_3BO_3, 0.093 μM $CuCl_2 \cdot 2H_2O$, 0.191 μM $ZnSO_4 \cdot 7\ H_2O$, 0.031 μM $Na_2MoO_4 \cdot 2\ H_2O$, 0.015 μM $VoSO_4$, and 0.016 μM $CoSO_4$ [25] . PLFE lipids were isolated from *S. acidocaldarius* cells as described [23] .

3.3 Isolation of S. acidocaldarius microvesicles (Sa-MVs)

MVs were isolated via ultrafiltration and ultracentrifugation of *S. acidocaldarius* supernatant. Briefly, supernatant of cell suspensions was col- lected and subject to a low

speed centrifugation (10,000 ×g) for 20 min using a Sorvall SLA-3000 rotor in a Sorvall RC5B Plus centrifuge to remove whole cells and large cellular debris. The resulting supernatant was concentrated in a Millipore ultrafiltration unit through a membrane with a 100 kDa molecular weight cut-off. Concentrated supernatant was then centrifuged at 126,000 ×g for 45 min using a Sorvall T-875 rotor in a Beckman L7 ultracentrifuge. 3/4 of the supernatant was discarded and the resulting pellet (containing MVs) was re-suspended in the residual supernatant. The MVs were then centrifuged at 19,000 ×g in the same ultracentrifuge to remove remaining larger vesicles and cellular debris. The resulting supernatant was kept and centrifuged a final time at 374,000 ×g to isolate MVs, which were resuspended in either final growth media, or 50 mM Tris buffer (10 mM EDTA, 0.02% NaN_3, pH 7.2) or 50 mM sodium phosphate/citrate buffer (10 mM EDTA, 0.02% NaN_3 , pH 2.6) or 50 mM citric acid solution (pH 2.6) and stored at room temperature. This procedure is outlined in Table 1.

Step	Method; Rotor/Centrifuge	G force	rpm	Time (min)	Collect
1	Sorvall SLA-3000/ Sorvall RC5B Plus	11,000 x g	8,000	20	supernatant
2	ultrafiltration				concentrated supernatant
3	Sorvall T-875/ Beckman XL-90	126,000 x g	36,000	45	¼ supernatant and pellet
4	Sorvall T-875/ Beckman XL-90	19,000 x g	14,000	20	supernatant
5	Sorvall T-875/ Beckman XL-90	374,000 x *g*	62,000	60	Pellet (i.e., Sa-MVs)

Table 1: Steps involved in the isolation of Sa-MVs from the *S. acidocaldarius* cell suspensions

3.4 Extraction of lipids from Sa-MVs and formation of reconstituted liposomes

Lipids were extracted from Sa-MVs using a solvent mixture of chloroform, methanol and water (34.5:34.5:31, v/v/v). The solution was then vortexed constantly for 30 min and left to separate for several hours. The resulting mixture was separated into three distinct phases: an aqueous phase, an organic phase, and an interfacial region. Each phase was assayed for total phosphate content as well as total protein content using the Bartlett phosphate assay and Lowry protein assay, respectively (59). The organic phase was found to contain a large portion of the total phosphate from Sa-MVs, presumably from phospholipids. No protein was detected in the organic phase. The organic phase was first dried under a stream of nitrogen gas, followed by further drying overnight under high vacuum. The resulting dried lipid film was rehydrated with a buffer solution and vortexed at 70 ˚C to make multilamellar vesicles (MLVs). The MLVs were then extruded (Lipex Biomembranes, Vancouver, Canada) 10 times through two 200-nm Nucleopore polycarbonate membranes at 70 ˚C to create large unilamellar vesicles (LUVs). LUVs of the bipolar tetraether lipid PLFE and the diester lipids 1-palmitoyl-2-oleoyl-*sn*-glycero-3-phosphocholine (POPC), dipalmitoyl-*sn*-glycero-3-phosphocholine (DPPC) and dimyristoyl-*sn*-glycero-3-phosphocholine (DMPC) (Avanti Polar Lipids) were generated by the same extrusion method with the extrusion temperature at ~70 ˚C for PLFE and ~50 ˚C for diester lipids.

3.5 Measurements of particle size, polydispersity, and zeta potential

The size and size distribution of Sa-MVs and reconstituted liposomes in either buffer or final growth media were determined by dynamic light scattering on either a Malvern Zetasizer Nano ZS or a Malvern Zetasizer 1000HS spectrometer (Wores, UK). Hydrodynamic diameter (Z avg) was calculated using the Stokes-Einstein equation. The size distribution was evaluated based on the polydispersity index (PDI). Zeta potential was measured on the Malvern Zetasizer Nano ZS spectrometer using laser Doppler electrophoresis.

3.6 Electron microscopy

Morphology of Sa-MVs and the reconstituted liposomes were ex- amined by negative staining-cryo transmission electron microscopy. Aliquots (5 microliter) of Sa-MVs or reconstituted liposomes in buffer and 1% ammonium molybdate solution (1:1, v/v) were pipetted onto a carbon coated 200-mesh copper grid. Excess liquid was removed by ad- sorption using Whatman No. 1 filter paper at the edge of the grid. The grid was then allowed to air dry for 60 s before being flash frozen in liquid ethane by using a home-made plunger, and then cooled in liquid nitrogen. Images were captured using a JEOL JEM-1400 transmission electron microscope equipped with a GATAN model 626 single tilt liq- uid nitrogen cryo transfer holder (at 80 kV) and processed using software from GATAN and Image J.

3.7 Autoclaving

The liposomes or Sa-MVs were dispersed in 50 mM citric acid solution (pH 2.6) or 50 mM Tris buffer (pH 7.2) and placed in a Pyrex test tube loosely covered by a screw cap, allowing the pressurized steam in the autoclave to reach the vesicles. In each autoclaving cycle, vesicles were autoclaved by the LS Gravity Steam Sterilizer (model 522, Getinge, Rochester, NY) for 20 min at 121 ˚C under a steam pressure of 18 psi. Lipid vesicles and Sa-MVs were stored at room temperature for at least one hour between consecutive autoclaving cycles. Prior to the size or TEM measurements, the autoclaved vesicles were stored at room temperature for at least one hour.

3.8 Chemicals and reagents

Stock solution (70 μM) of Laurdan (Avanti Polar Lipids) was made in N,N'-dimethylformalaminde (DMF, Sigma-Aldrich, St. Louis, MO). Stock solution (40-80 mM) of n-tetradecyl-β-D-maltoside (TDM, Sigma-Aldrich) was prepared in deionized water. The concentrations of POPC, DMPC, and PLFE stock solutions were determined by the method of Bartlett. The concentration of SA-MVs is expressed in terms of the total protein content as determined by the Lowry assay (59).

3.9 Spectroscopy measurements

Emission and excitation spectra were measured using an ISS K2 fluorometer (Champaign, IL). Temperature of the samples in the cuvette was controlled using a circulating water bath and measured by a thermal couple. Excitation spectra of intrinsic

protein fluorescence were measured using a ratio mode based on the emission intensity monitored at 315 nm through an emission monochromator (slit-width = 4 nm) over the intensity measured from rhodamine B in ethylene glycol (3 mg/mL) plus a RG630 filter in the reference channel. Technical emission spectra (as opposed to the corrected emission spectra) of intrinsic protein fluorescence were measured using the excitation light at 275 nm with both emission and excitation monochromators set at 8 nm. For the extrinsic membrane probe studies, Sa-MVs, LUV_{PLFE} and LUV_{MVs} were incubated with aliquots of Laurdan (in DMF) with stirring at ~65°C for 2 h, whereas LUV_{DPPC} and LUV_{POPC} were doped with Laurdan with stirring at ~50°C for 1 h. The probe-to-lipid molar ratio was ~1/400 for LUV_{PLFE}, LUV_{DPPC} and LUV_{POPC}. The probe content in Sa-MVs was 0.29 nmol of Laurdan per μg of protein. The technical emission spectra of Laurdan in Sa-MVs and various liposomes were recorded from 370 nm to 600 nm or from 408 nm to 600 nm using excitation at 340 nm or 390 nm, respectively. The background readings from Sa-MVs or liposomes without the probe were subtracted from the sample readings. All the emission spectra presented in this study are technical emission spectra.

The excitation GP was calculated from the resulting emission spectra using the equation: $GP= (I_{440} – I_{490})/(I_{440} + I_{490})$. Here I_{490} and I_{440} are the fluorescence intensities at 490 and 440 nm, respectively. To obtain the Laurdan's red edge excitation shift (REES) value, the wavelength-based emission spectra were converted to the wave number-based spectra. The REES value was determined by subtracting the center of mass of Laurdan's wave number-based emission spectra excited at 340 nm from that excited at 390 nm.

Absorption spectra were measured on an OLIS CLARiTY 1000A spectrophotometer (OnLine Instrument Systems, Bogart, GA) as described (60). This instrument is a novel integrating cavity absorption meter able to conduct accurate absorbance measurements in particle suspensions that scatter light. Identical 8-ml solutions of 20 mM Tris buffer with 10 mM EDTA and 0.02% (w/v) sodium azide were added to both the sample and reference observation cavities of the spectrophotometer. After recording a stable baseline, a volume was withdrawn from the sample cavity and replaced with an equal volume of suspended microvesicles. The contents of both observation cavities were maintained at 25^{o} C using a model TC-1 Peltier temperature control element from Quantum Northwest (Liberty Lake, WA, USA). Raw absorbance spectra were collected at a rate of 6.2 scans over the wavelength range per second for two minutes, and the resulting spectra were averaged. These averaged raw absorbance values were subsequently converted to equivalent absorbance values per cm using Fry's method (60) with analysis software provided by OnLine Instrument Systems.

3.10 Generation of free standing planar membranes

Recordings were obtained using a horizontal bilayer chamber at 22–24°C. Solution in the cis (top) chamber contained 200 mM KCl and 10 mM HEPES, pH 6.8, with no added Ca^{2+}. Solutions in the trans (bottom) chamber contained 200 mM KCl and 10 mM HEPES, $CaCl_2$ added to reach the indicated concentrations, at pH 7.6. The solution on the cis side of the membrane (pH 6.8 and with no added Ca2+) suppressed the activity of MthK channels that were incorporated with their cytoplasmic face toward the cis chamber to

nominal levels (92), resulting in the activation only of MthK channels with their cytoplasmic end facing the trans chamber. After the addition of the trans well buffer, Clear transparency poked with a pin to create a pore was pre-treated with lipid dissolved in decane and left to air dry for 10 minutes. The cis chamber was then filled and planar membranes formed spontaneously across the pinhole. If unsuccessful, the suspended lipid was agitated slightly by mechanical force of a small air bubble generated from the tip of a pipette. Membrane generation was monitored by capacitance measurements.

3.11 Statistical analysis

Data are expressed as mean ± standard deviation. In order to ascertain statistical significance, a Student's paired *t* -test was used to compare experimental groups of microvesicles to the unaltered or basal population. Analysis was completed using Microsoft Excel version 2016. P values less than 0.02 are denoted by an asterisk.

CHAPTER 4: RESULTS

CHARACTERIZATION OF *S. ACIDOCALDARIUS* MICROVESICLES

4.1 Long-term stability of Sa-MVs

The long-term stability of the isolated Sa-MVs stored in Tris buffer (pH 7.2) at ~22$_o$C was examined by measuring the particle size, polydispersity (PDI), and zeta potential (ZP) at 25 ˚C over several months (Figure 2). The average size increased by ~50 nm in the first 14 days ($p < 0.02$, $n = 3$), probably due to subtle particle aggregation. Thereafter, the size remained almost constant in the time course 14-137 days. Over such a long time period, the PDI values remained low (0.15-0.3), whereas zeta potential fluctuates within a narrow range −4-8 mV. Overall, these data showed that Sa-MVs in Tris buffer exhibited long-term stability, with no signs of vesicle disintegration or a large scale vesicle aggregation or vesicle fusion.

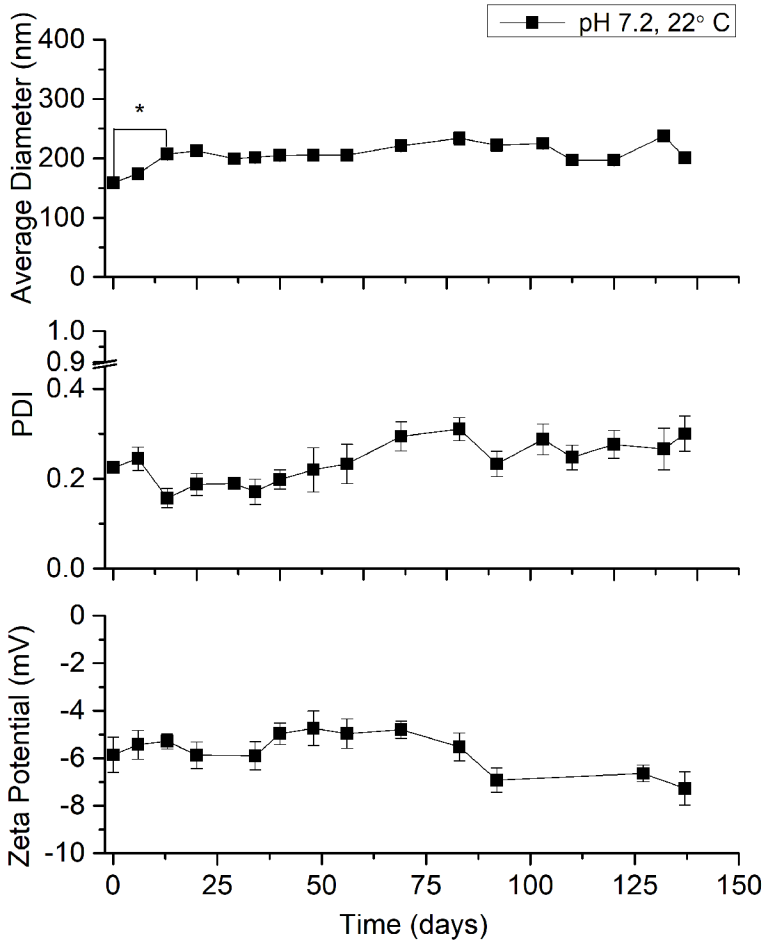

Figure 2. Long term stability of Sa-MVs. Particle diameter (top), polydispersity (PDI, middle), and zeta potential (bottom) of Sa-MVs in 50 mM Tris buffer (pH 7.2) containing 10 mM EDTA and 0.02% NaN_3, were monitored over several months. The error bars, which are smaller than the symbols in the case of average diameter (top), are the standard deviations from three measurements. A Student's *t* test was used to compare size values recorded at day 0 to those recorded at day 13. The asterisk denotes $p < 0.02$.

4.2 Sa-MV stability against temperature and pH

The top panel of Figure 3 shows the temperature dependence of particle size, PDI, and zeta potential of Sa-MVs in the growth media that we have used to grow *S. acidocaldarius* cells. The PDI values remained low (≤ 0.15) at all the temperatures and pHs examined, which indicates that the size distribution is considerably homogenous, irrespective of the temperature and pH. At pH 7.2, the vesicle size changed little with temperature over the temperature range (25-80 ˚C) examined in both the heating and cooling mode. At pH 2.6, there is a slight increase (9 nm, $p < 0.02$) in vesicle size with increasing temperature from 25 to 80 ˚C, while the temperature dependence of the particle size is reversible upon cooling. This size increase is probably due to increased aggregation caused by a slight decrease of pH in the growth medium with increasing temperature (−0.013 pH unit per degree). Based on the data given in Figure 3, it can be claimed that at the cells' growth pH (2.6) and growth temperature (75 ˚C), the average Sa-MV size is ~180 nm in diameter and that, when the pH of the growth media is changed from 2.6 to 7.2 while the growth temperature remains at 75 ˚C, the size of Sa-MVs drops to ~136 nm. Similar temperature and pH effects on particle size and PDI were observed when Sa-MVs were dispersed in 50 mM Tris buffer (pH 7.2) or 50 mM citric acid solution (pH 2.6) (bottom, Figure 3). In these buffers, MV size and PDI changed very little with temperature. When the pH of the buffer was increased from 2.6 to 7.2, the Sa-MV size was decreased by ~40 nm, comparable to that seen in the growth media (top panel, Figure 3). Thus, the pH-induced change in particle size seems to occur independent of the type of the solution around the Sa-MVs. The zeta potential of Sa-MVs changes significantly with pH,

decreasing from −0.5 mV at pH 2.6 to −5 mV at pH 7.2 in the cell growth media (top, Figure 3) or from −1 mV at pH 2.6 to −9-10 mV at pH 7.2 in buffer solutions (bottom, Figure 3). These size and zeta potential changes with pH could be due to the changes in the orientation of the S-layer proteins (61), the conformational change of the polar headgroups of tetraether lipids (62) and/or the change in the degree of protonation of amino acids on the Sa-MV surface proteins and of the tetraether lipid polar headgroups.

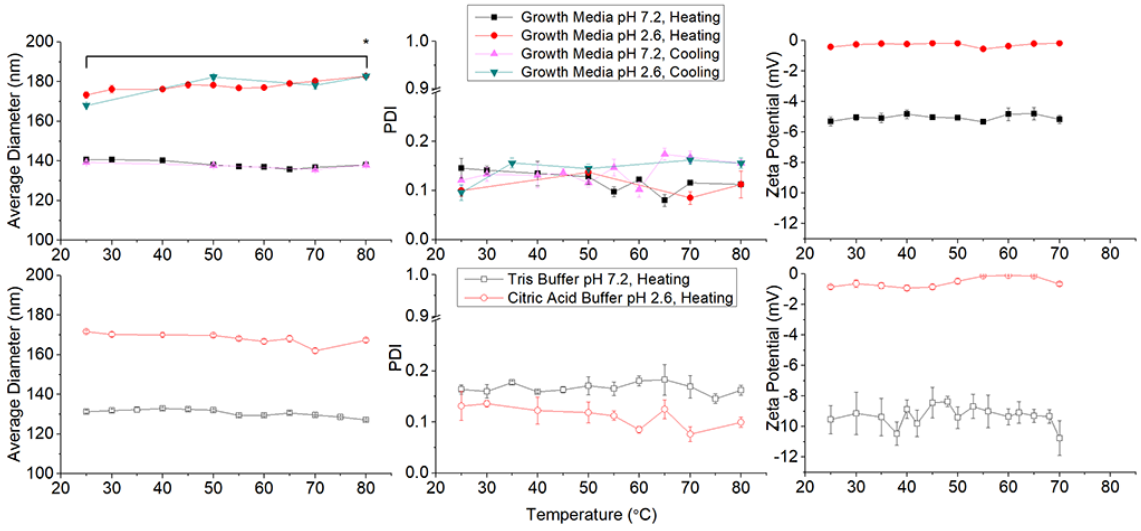

Figure 3. Temperature dependence of the average particle size, PDI, and zeta potential of Sa-MVs. Sa-MVs were dispersed in (top) growth media and (bottom) Tris (pH 7.2) or citric acid (pH 2.6) buffer. All the Sa-MVs used in the growth media studies were obtained from the same batch of MV preparation, and all the Sa-MVs used in the buffer solution studies were obtained from another same batch. Buffer: 50 mM Tris containing 10 mM EDTA and 0.02% NaN3 (pH 7.2) or 50 mM citric acid containing 0.02% NaN_3 (pH 2.6). The asterisk denotes $p < 0.02$.

The results shown in Figure 3 prompt us to do a more detailed study on the pH dependence of Sa-MV's size/PDI in a simpler medium, i.e., 1 mM KCl (Figure 4). In this experiment, the pH was changed by small increments from neutral to low pH by using 0.1 M HCl and then the reversibility of the pH effect was examined from low pH to neutral by using 0.1 M NaOH. The results (Figure 4) show that there is a steady increase in both particle size and PDI when the pH of 1 mM KCl is changed from 4.3 to 3.0. The size and PDI changes are reversible, which suggests that the size increase at low pH is probably not due to the removal of S-layer proteins, which would most likely cause an irreversible decrease in particle size. The small increase in PDI from 0.1 at pH 4.3 to 0.22 at pH 3.0 (Figure 4) may be caused by subtle particle aggregation due to a decrease in the absolute value of the zeta potential (Figure 3) and hence a reduction in particle-particle repulsion. The reversible nature of the pH-induced change in particle size and PDI also suggests that the aggregation, if it occurs, is not followed by vesicle fusion, which would be irreversible. Aggregation that is not followed by fusion is a result typical for tetraether lipid-based vesicles (63).

In order to determine if the increase in Sa-MV particle size at low pH is due to conformational changes of S-layer proteins or tetraether lipid headgroups, we used liposomes reconstituted from Sa-MV lipids to conduct an experiment similar to that shown in Figure 4. In the reconstituted liposomes, where proteins are removed, there is no difference in liposome size and PDI between neutral pH and pH 2.6 in both high-to-low pH and low-to-high pH mode (Figure 5). These results strongly suggest that the rise in particle size and PDI observed in Sa-MVs (Figures 3 and 4) at low pH comes from

conformational changes of Sa-MV S-layer proteins, not from tetraether lipids, and the protein conformational changes may occur in concomitant with subtle vesicle aggregation as discussed earlier.

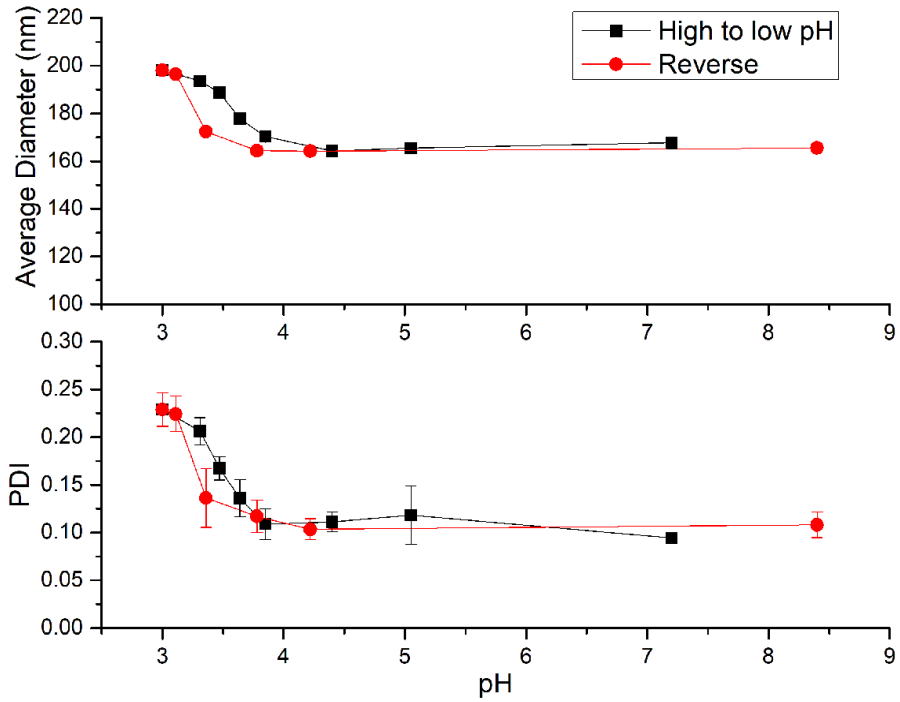

Figure 4. Effects of pH on the particle size and PDI of Sa-MVs in 1 mM KCl at room temperature (~22₀C). Error bars are the standard deviations from three measurements.

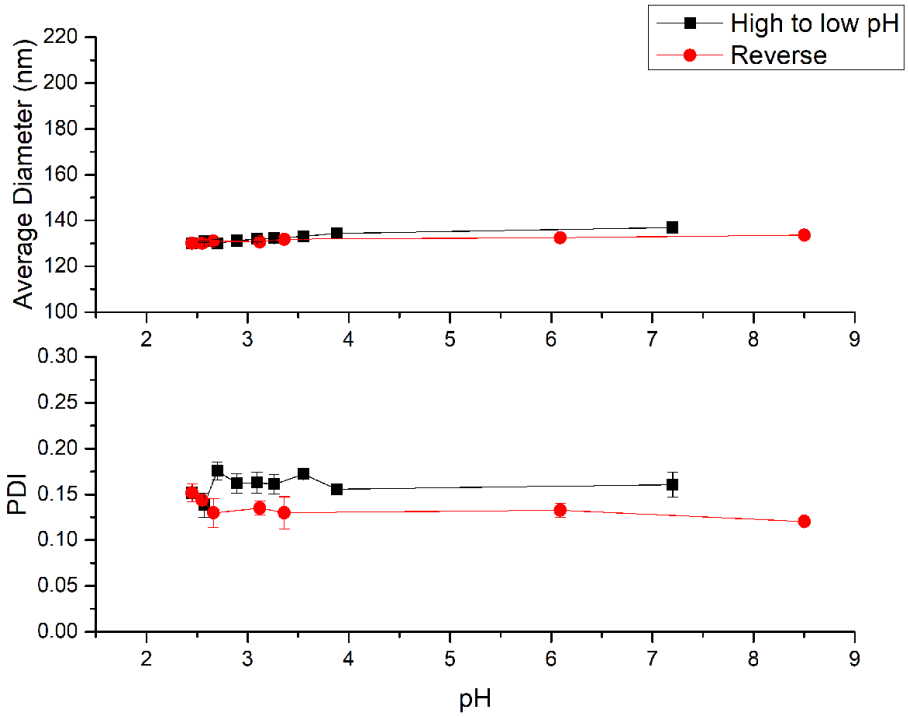

Figure 5. Effects of pH on the particle size and PDI of LUVMV. LUVMVS were dispersed in 1 mM KCl at room temperature (~22oC). Error bars are the standard deviations from three measurements.

Effects of pH on the zeta potential of Sa-MVs and liposomes reconstituted from Sa-MV lipids in 1 mM KCl are presented in Figure 6. It can be determined from Figure 6 that the isoelectric point (pI) for Sa-MVs is 3.0 while that for the reconstituted liposomes (LUV_{MV}) is estimated to be below 2.0 (Figure 6). The pH dependence of zeta potential is very different between these two samples. In the case of Sa-MVs, zeta potential increases monotonically with decreasing pH. In the case of LUV_{MV}, there is a biphasic change in zeta potential at pH 3.5; below pH 3.5, there is a sharp increase in zeta potential with decreasing pH. These data suggest that, like PLFE lipids, the tetraether lipids in Sa-MVs are highly negatively charged at pH 3.5-7.2 and that this negative surface charge is diminished when the S-layer proteins are present. The pI value equal to 3.0 indicates that at this pH the charge-charge repulsion between Sa-MV particle is the least, which also explains why the particle size of Sa-MVs increases to a maximum at pH 3.0 (Figure 4). In other words, at this low pH, Sa-MVs may undergo some degree of aggregation, in conjunction with the S-layer protein conformational changes, which lead to an increase in particle size (Figure 4).

Next, native Sa-MVs and LUV_{MV} at pH 7.2 and 2.6 were examined by cryo-transmission electron microscopy (TEM) in order to find evidence for particle aggregation, confirm the particle size increase at low pH, and study the effect of pH on particle morphology. Figure 7 shows that LUV_{MV}s are not as spherical as Sa-MVs and that the size of individual Sa-MVs at pH 2.6 is significantly larger than that at pH 7.2 whereas the size of LUV_{MV} changes little between these two pHs, which is consistent with the light scattering data (Figures 3 and 4). These TEM images suggest that the size increase in

individual Sa-MVs with lowering pH (Figures 3 and 4) can be attributed to the presence of proteins, most likely, the S-layer proteins. At pH 2.6, we observed aggregation of Sa-MVs in some areas of the EM images (illustrated in Figure 7), in coexistence with non-aggregated Sa-MVs. Aggregation does not seem to occur for reconstituted liposomes.

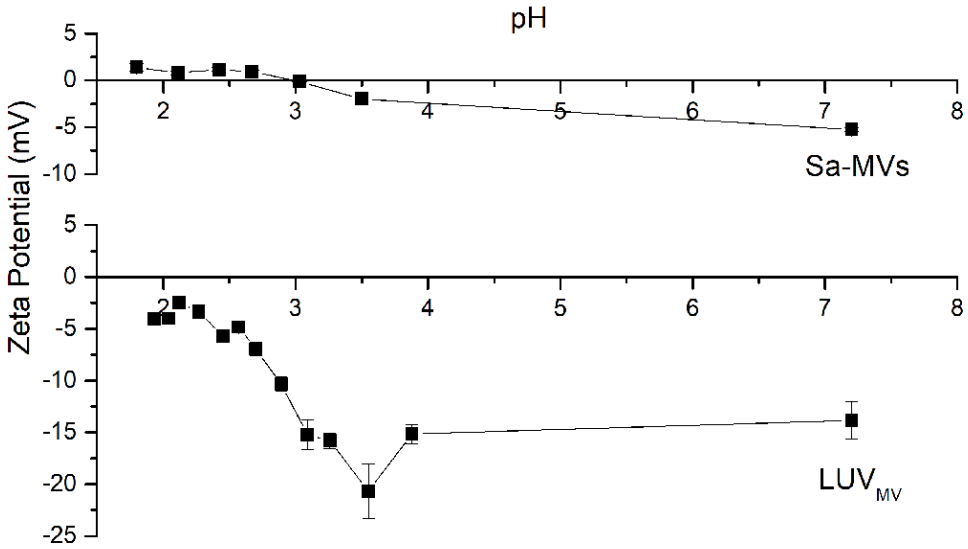

Figure 6. Effects of pH on the zeta potential of Sa-MVs and LUV$_{MV}$. Sa-MVs and LUV$_{MV}$ were dispersed in 1 mM KCl at room temperature (~22^{o}C). Error bars are the standard deviations from three measurements.

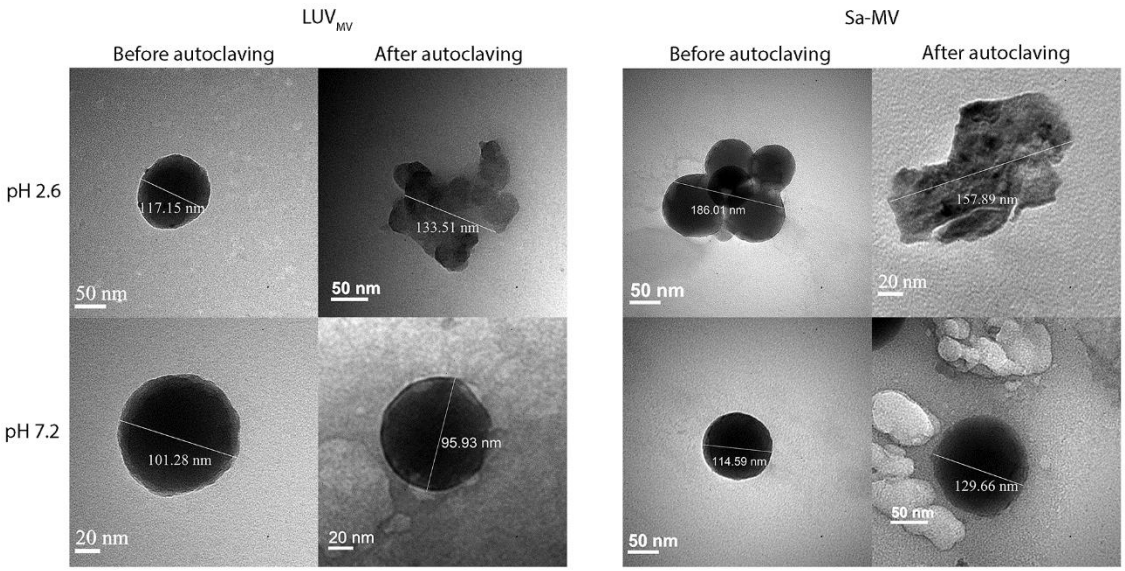

Figure 7. Negative staining cryo-TEM images of Sa-MVs and LUVMV. Representative negative staining cryo-TEM images of Sa-MVs and LUVMV at pH 2.6 and pH 7.2 before and after one cycle of autoclaving are presented. Buffers used: 50 mM Tris, 10 mM EDTA, 0.02% NaN_3, pH 7.2 and 50 mM citric acid, 0.02% NaN_3, pH 2.6.

4.3 Sa-MV stability against autoclaving

Autoclaving is one of the most effective pathogen decontamination methods for liposomes (64) . The ability to maintain particle integrity after autoclaving would be a desirable feature for systemic use of Sa-MVs. Previous studies showed that liposomes made of bipolar tetraether lipids such as PLFE can sustain autoclaving at neutral pH (65). Since Sa-MVs contain exclusively tetraether lipids and the membrane of Sa-MV is covered by a crystalline S-layer (23), it is expected that Sa-MVs can sustain autoclaving as well. Indeed, our light scattering data (Figure 8) show that the particle size of Sa-MVs, LUV_{MV}, and LUV_{PLFE} dispersed in buffer at pH 7.2 changes little over five consecutive autoclaving cycles while liposomes made of diester lipids such as POPC and DMPC cannot sustain more than three or four cycles of autoclaving at pH 7.2 (Figure 8). At pH 2.6, the stability against autoclaving is reduced for all vesicles examined. At pH 2.6, Sa-MVs and LUV_{MV} show a significant increase in particle size after one cycle of autoclaving whereas LUV_{POPC} and LUV_{DMPC} show not only a size increase after the first autoclaving cycle, but also a large scale of aggregation after the second autoclaving cycle. These results are consistent with the previous finding that sterilization of diester liposomes by autoclaving is limited to neutral pH (64). At low pHs, lipid hydrolysis and oxidation may occur to diester liposomes during autoclaving, leading to liposome aggregation and/or a significant loss of entrapped materials (64). For all the tetraether lipid-based vesicles examined, LUV_{PLFE} appears to be the most stable against autoclaving at both pHs and shows a sign of size increase only after four autoclaving cycles at pH 2.6. The images of cyro-TEM (Figure 7) showed that, at pH 2.6, after one cycle of autoclaving the morphology of Sa-MVs and LUV_{MV} has actually

been changed from spherical to an irregular shape (Figure 7). Taken together, it can be concluded from light scattering and TEM data that Sa-MVs are stable against multiple autoclaving cycles at neutral pH (Figures 7 and 8).

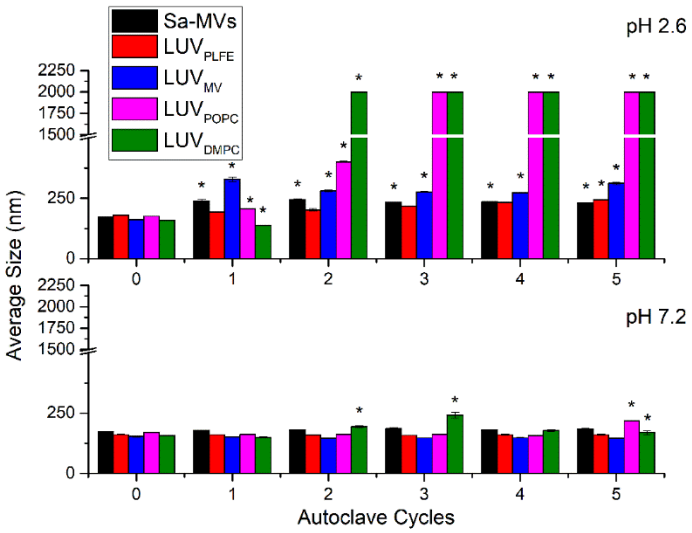

Figure 8. **Stability of Sa-MVs and various LUVs against autoclaving.** The measurements were made in 50 mM citric acid buffer (pH 2.6) containing 0.02% NaN_3 or 50 mM Tris buffer (pH 7.2) containing 0.02% NaN_3. Asterisk indicates a p value < 0.02 (n =3) when autoclaved vesicle groups were compared with native (unautoclaved) groups.

4.4 Sa-MV stability against the detergent Triton X-100

The potential application of Sa-MVs is not limited to nanomedicine. Because of their great stability over a wide range of temperatures and pHs, Sa-MVs could also be engineered to become an extraordinarily stable platform suitable for biosensing, biocatalysis, and artificial photosynthesis in both ambient and harsh conditions. Thus, it is of interest to test the stability of Sa-MVs against other environmental stressors such as surfactants. Figure 9 shows the effect of the surfactant Triton X-100 on the particle size of Sa-MVs in comparison to the results from unilamellar vesicles made of Sa-MV lipids (LUV_{MV}), bipolar tetraether lipids PLFE extracted from *S. acidocaldarius* (LUV_{PLFE}), diester lipid DPPC (LUV_{DPPC}), and diester lipid POPC (LUV_{POPC}).

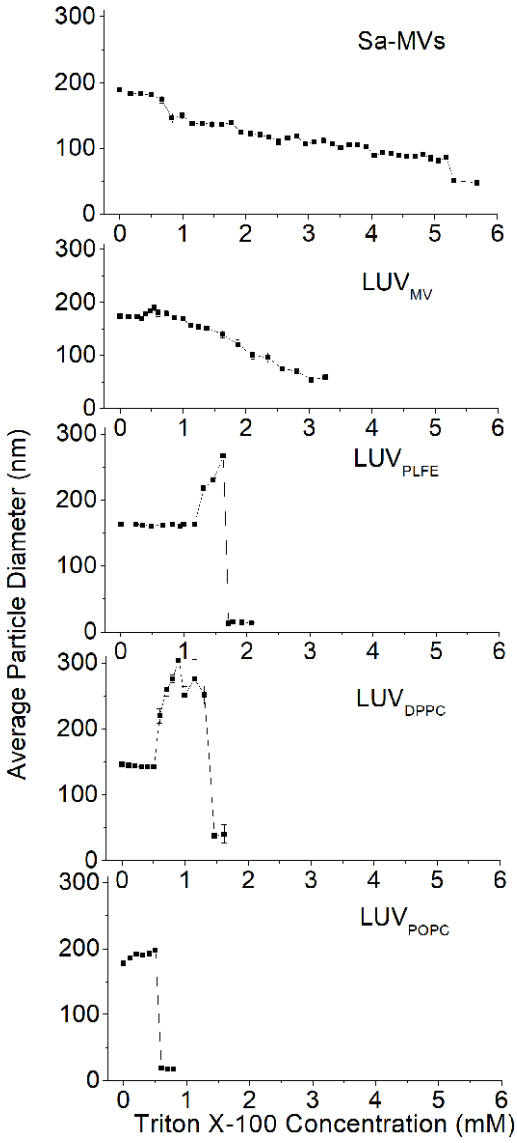

Figure 9. Stability of Sa-MVs and various unilamellar vesicles (LUVs) of lipids against the surfactant Triton X- 100. All samples were suspended in 50 mM Tris buffer containing 10 mM EDTA and 0.02% NaN_3 at pH 7.2. Measurements were conducted at 25 C and error bars were the standard deviations from three measurements. All the samples were compared based on the same amount of lipids.

The profiles of vesicle diameter versus Triton-X-100 concentration for LUV_{PLFE}, LUV_{DPPC} and LUV_{POPC} are consistent with the three-stage model for surfactant-lipid membrane interactions (66). The first stage is surfactant insertion into membranes, which leads to an increase in particle size until reaching a maximum where the surfactant insertion is saturated. Thereafter, there is a drop in particle size due to formation of mixed micelles and vesicle disruption. In the final stage, the particle size levels off to a very low value which reflects a total solubilization of the vesicles and maximal micelle formation. In these profiles, the maximum vesicle diameter reflects the extent of resistance to surfactant-induced membrane disruption. We found that the critical Triton X-100 concentration (C_r) where the maximum vesicle diameter occurs is decreasing in this order: C_r (LUV_{PLFE}) > C_r (LUV_{DPPC}) > C_r (LUV_{POPC}). This trend makes sense because membrane packing tightness at room temperature (~22 ˚C) is known to also decrease in this order: PLFE > DPPC > POPC (67). In comparison, the profile of particle size versus Triton X-100 concentration for Sa-MVs and LUV_{MV} looks different. In the case of LUV_{MV}, there is no sharp decrease in size after the size reaches the maximal value at [Triton X- 100] ≈ 0.6 mM (Figure 9); instead, there is a gradual decrease in particle size in response to increased Triton X-100, which suggests that, for some reason, Triton X-100 micelles (critical micelle concentration = 0.22-0.24 mM, Sigma Data) cannot efficiently solubilize the lipids in LUV_{MV}. Similarly, in the case of Sa-MVs, Triton X-100 causes a gradual and stepwise, rather than a sharp, decrease in particle size (Figure 9). The stepwise decrease is probably due to the gradual removal of the S-layer by Triton X-100 (68). The lack of a sharp decrease suggests that

Triton X-100 micelles have some difficulties to disrupt the lipid membrane in Sa-MVs, as is the case seen in LUV$_{MV}$.

CHAPTER #5

RESULTS PART 2

5.1 Intrinsic protein fluorescence

The emission spectrum of the intrinsic fluorescence of Sa-MVs in Tris buffer freshly isolated from the cell suspensions is presented in Figure 10 (black curve, labeled as "undialyzed"). Three emission peaks (Peaks I, II and III) were detected at 316, 373, and 420 nm, respectively, when excited at 275 nm. After the dialysis (MWCO 25,000 kDa, Spectra/Por membrane, Spectrum, Houson, TX) of Sa-MVs against the same Tris buffer (1 mL sample versus 2 L buffer) for 4 h, the intensities of Peaks II and III were reduced significantly while the emission wavelengths of these two peaks did not shift (Figure 10, green curve). Additional dialysis against 2 L buffer with the buffer changed every four hours for 48 h further reduced the fluorescence intensities of Peak II and Peak III while Peak I remained as the dominating fluorescence peak of Sa-MVs (Figure 10, blue curve). The emission spectrum of the intrinsic Sa-MV fluorescence is virtually unchanged after 48 h of dialysis (Figure 10, red curve for 72 h dialysis).

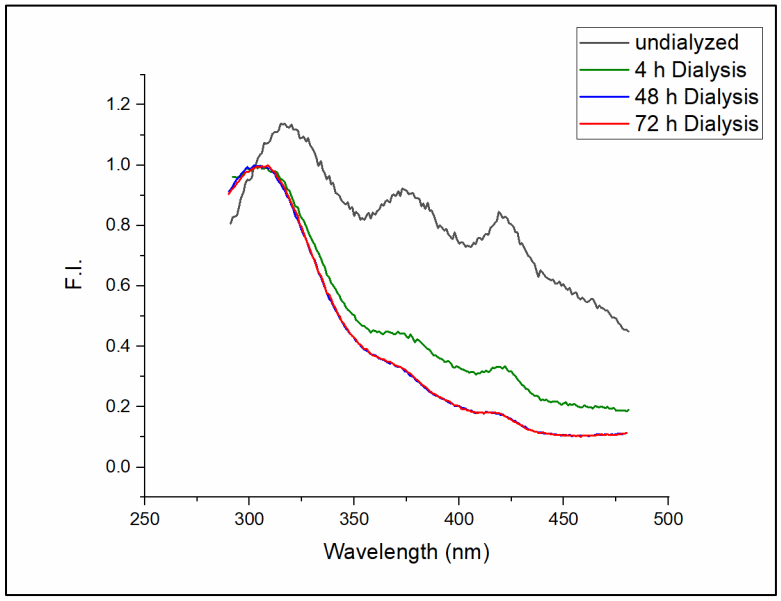

Figure 10. Effect of dialysis on the technical emission spectra of Sa-MVs isolated from *S. acidocaldarius* cell suspensions. λ_{ex} = 375 nm; slit-width = 8-nm for both the excitation and the emission monochromator; temperature = 23^{o}C.

Light at 275 nm excites both tryptophans and tyrosines in Sa-MVs. Based on the emission wavelengths at the peaks, it can be suggested that Peaks II and III in Figure 2 do not originate from tryptophans nor tyrosines in Sa-MV proteins. Since Peak II and III can be significantly reduced to a minimal level by dialysis, these two fluorescence peaks most likely come from some small molecules, either originally produced by the cells or inherited from the cell growth environment, that are loosely bound to Sa-MVs. Extensive dialysis can reduce but cannot completely eliminate these two fluorescent peaks, suggesting that these small molecules also have tight binding to Sa-MV membranes or some Sa-MV proteins. The particle size and the PDI value of Sa-MV do not change with dialysis (Table 2), indicating that those small molecules that are removed by dialysis are not S-layer proteins nor membrane lipids. A thorough investigation of the chemical identifies of Peaks II and III will be undertaken in the future and is beyond the scope of the current study. In the present study, we focus on Peak 1 (Figure 10) because we believe it originates from protein intrinsic fluorescence, which would bear more biological interests such as the structures and dynamics of protein folding and association.

Time Dialyzed (Hrs)	Particle Size (nm)	PDI
0	213.40 ± 0.79	0.187 ± 0.030
4	209.70 ± 1.57	0.176 ± 0.006
8	209.43 ± 1.97	0.185 ± 0.006
12	210.57 ± 1.63	0.185 ± 0.005
16	208.40 ± 2.46	0.186 ± 0.007
20	210.27 ± 2.54	0.192 ± 0.016
24	211.77 ± 6.09	0.179 ± 0.027
28	209.07 ± 2.76	0.181 ± 0.012

Table 2. Sa-MV size and poly dispersity index. Size and PDI as measured by dynamic light scattering over the course of 28 hours of dialysis

.

Extensive dialysis caused the apparent emission maximum of Park I to shift from 316 nm to 303 nm (Figure 2). Intrinsic protein fluorescence peaked around 303 nm is rare, which requires some discussion. Intrinsic protein fluorescence mainly comes from tryptophans and tyrosines. Since tyrosine has an extinction coefficient four times lower than tryptophan and since tyrosine fluorescence is often quenched in the protein by a variety of mechanisms including energy transfer to tryptophans, tryptophan usually dominates intrinsic protein fluorescence (69). A prominent example is bovine serum albumin (BSA), which has 18 tyrosines and 2 tryptophans. While tryptophan takes up only 10% of the fluorescent aromatic amino acids (disregarding phenylalanine due to its low extinction coefficient and fluorescence quantum yield), the emission spectrum of BSA in solution is dominated by tryptophans, showing a maximum fluorescence intensity at 345 nm (70).

The fluorescence emission spectrum of dialyzed Sa-MVs shown in Figure 2 is an exception, similar to the case of the bacterial elongation factor Tu (71), to the general trend that tryptophan dominates intrinsic protein fluorescence. Sa-MVs have 29 distinct proteins and most, if not all, Sa-MV proteins contain multiple tryptophans and tyrosines (23). The most abundant protein species in Sa-MVs are the S-layer proteins (23), namely, SlaA and SlaB (27). SlaA from *S. acidocaldarius* contains 96 tyrosines and 6 tryptophans (72). To our knowledge, the amino acid composition of SlaB from *S. acidocaldarius* has not been reported yet, however, SlaB from a similar thermoacidophilic archaeon *Sulfolobus solfactaricus* contains 16 tyrosines and one tryptophan (73). Since about 95% of the

fluorescent aromatic amino acids in the S-layer proteins are tyrosines and since the fluorescence of free tyrosine in solution at neutral pH has an emission maximum at 303 nm (74), it is not unreasonable to observe that the emission maximum of dialyzed Sa-MVs occurs at 303 nm when excited at 275 nm (Figure 2). In this case, unlike the case of BSA (70), tyrosines in Sa-MVs are not quenched.

A tightly packed protein matrix in Sa-MVs near tyrosine and tryptophan residues could be another plausible explanation for the observation of the emission maximum at the low wavelength 303 nm. One precedent is the fluorescence of *Pseudomonas fluorescens* azurin, which has an emission maximum at 305-308 nm when excited at 275 nm (75). *Pseudomonas fluorescens* azurin is a single tryptophan protein, and its low wavelength for emission maximum has been attributed to the apolar environment surrounding the tryptophan residue, which is almost completely shielded from water (76). It is possible that most of the aromatic amino acid residues in Sa-MVs are also in a tightly packed, water-shielded protein matrix, thus giving a low wavelength for the emission maximum. Unlike azurin, which is molecularly dispersed in solution, S-layer proteins, the most dominant proteins in Sa-MVs, aggregate at the particle surface and are supposed to form regular crystalline lattices as they do on the surface of the archaea cells. In addition, some other proteins in Sa-MVs may also be anchored in the membrane located under the S-layer. At this end, it is of interest to test if there is spectroscopic evidence for the chromophores of the aromatic amino acid residues in Sa-MV proteins (mainly S-layer proteins) to from H- or J-aggregates.

We have used the surfactant n-tetradecyl-β-D-maltoside (TDM) as a tool to investigate the spectral difference in intrinsic protein fluorescence between native Sa-MVs (aggregation of S-layer proteins) and microvesicles completely disrupted by TDM (dis-aggregation of S-layer proteins). The critical micelle concentration (CMC) of TDM is 0.015 mM at 20^{o}C (77). As shown in Figure 3 (top), the particle size of dialyzed Sa-MVs increases by ~100 nm from 0 to ~0.2 mM TDM, which probably reflects the insertion of the surfactant into the vesicle membrane, according to the three-stage model of the surfactant-membrane interactions (78,79). At ~0.2 mM, TDM insertion reaches the limit. Thereafter, mixed micelles are formed, and vesicle disruption occurs, eventually leading to small fragments of 20-30 nm at high [TDM] (Figure 11). A similar trend was seen in our previous study of Sa-MVs against the surfactant Triton X-100 (42).

The bottom panel of Figure 11 shows that there are significant differences in spectral properties between Sa-MVs in the absence of TDM and presence of 10.13 mM TDM. In the absence of TDM, the emission maximum of Sa-MVs appears at 303.5 nm and the excitation maximum is at 288 nm. At [TDM]= 10.13 mM, the emission max appears at 312 nm and the excitation maximum is at 280.5 nm. There is a red shift by 7.5 nm in the excitation spectrum and an increase in excitation band sharpness, with the width of half maximum changed from 22.2 nm to 9.3 nm, when S-layer proteins are changed from the dis-aggregated state ([TDM] =10.13 mM) to the aggregated state ([TDM] = 0) (Figure 11).

The red shift, in conjunction with an increase in excitation band sharpness, is indicative of the occurrence of J-aggregates (80,81). In J-aggregates, molecules are paralleled aligned, with the transition dipole moments of the chromophore coherently coupled, resulting in

delocalization of electronically excited states over many (typically 3−50) monomeric chromophores (81,82). When forming J-aggregates, the excitation energy level is lowered and as a result the excitation/absorption band undergoes a red shift.

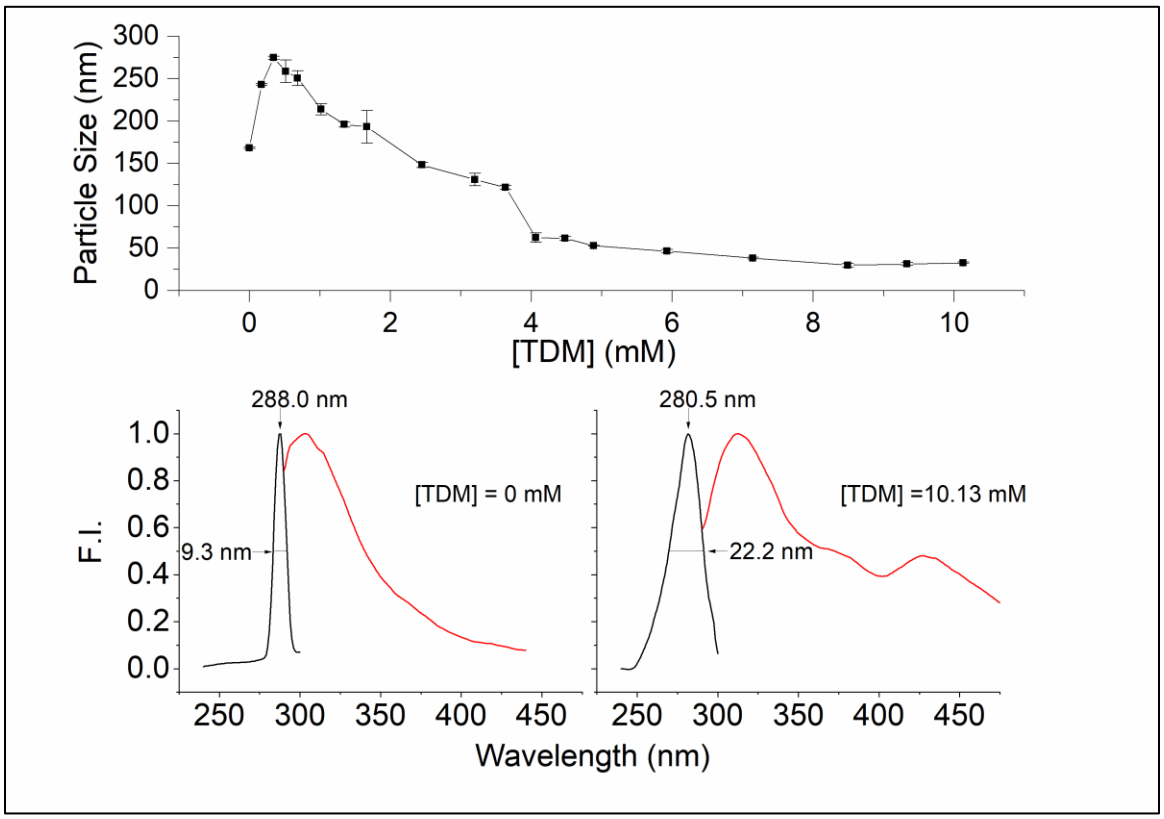

Figure 11. (*top*) The effect of TDM on the particle size of Sa-MVs in 50 mM Tris containing 10 mM EDTA and 0.02% NaN_3 (pH 7.2). Temperature = 23°C. (*bottom*) The excitation (black) and technical emission (red) spectrum of Sa-MVs in the absence of TDM (left) and in the presence of 10.13 mM TDM (right). The samples contained 36.8 micrograms of Sa-MV proteins/mL. Fluorescence intensities of the excitation spectra were recorded at 315 nm through an emission monochromator with a 4-nm slit-width, and the exciting light was selected via an excitation monochromator with an 8-nm slit-width. For the emission spectra, the excitation was fixed at 275 nm and the emission was measured through a monochromator with an 8-nm slit-width.

Absorption measurements of Sa-MVs (Figure 12) yielded the results consistent with those obtained from fluorescence measurements (Figures 10 and 11). Figure 12 (curve a) shows that the major absorption band of un-dialyzed Sa-MVs peaked at 287 nm, with a broad shoulder in the region 310-390 nm. This broad shoulder is significantly reduced after 72 hours of dialysis against buffer (curve b, Figure 12). The dialyzed Sa-MVs in the absence of TDM exhibit an absorbance maximum at 288 nm (curve b, Figure 12). In the presence of 11 mM TDM, when the S-layer proteins are dis-aggregated, the absorption maximum of dialyzed Sa-MVs is shifted to a shorter wavelength, 285 nm (curve c, Figure 12), similar to the trend observed in Figure 11. The excitation spectra shown in Figure 11 are sharp because they were determined by measuring the fluorescence intensity at 315 ± 8 nm, which monitored only the intrinsic protein fluorescence. In contrast, the protein absorption spectra shown in Figure 12 were relatively broad due to the presence of non-protein "impurities" (i.e., those responsible for Peaks 1 and 2 in Figure 10).

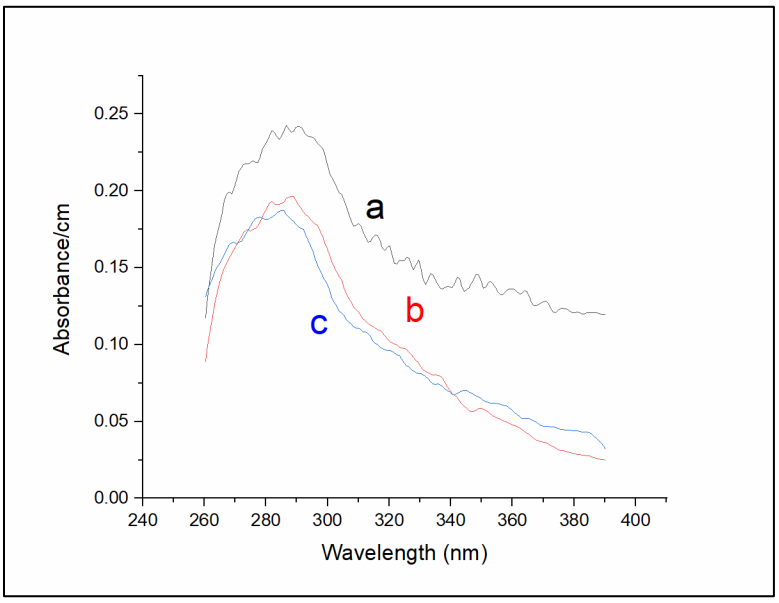

Figure 12. Absorption spectra of undialyzed Sa-MVs. (a), Sa-MVs after 72 h dialysis (b), and dialyzed Sa-MVs in the presence of 11 mM TDM (c), measured at room temperature.

Figures 13A and 13B show that the emission maximum of Sa-MVs in Tris buffer decreases monotonically and significantly with increasing temperature, changing from 303-305 nm at 20^{o}C to 296 nm at 75.4^{o}C. This temperature-induced blue shift is reversible upon cooling. A similar blue shift in $\lambda_{em,max}$ was observed (Table 3) when Sa-MVs were dispersed in 50 mM pyrophosphate buffer (pH 7.2). This test excludes the possibility that the blue shift in $\lambda_{em,max}$ shown in Figure 13B comes from the pH change due to the use of Tris buffer as the temperature dependence of pH is much less in pyrophosphate buffer than in Tris buffer.

This 7-9 nm blue shift in emission maximum (Figure 13B) is an interesting observation because elevated temperature usually unfolds the proteins, increases protein volume fluctuations, and makes aromatic amino acid residues more exposed to aqueous phase, which would lead to a red shift in emission maximum. Apparently, these did not happen to proteins in Sa-MVs. It is likely that the majority of the proteins in Sa-MVs (i.e., S-layer proteins) are retained in a very tightly packed situation over the entire temperature range examined (20-75^{o}C). This assertion is reasonable as liposomal membranes made of bipolar tetraether lipids have been shown to exhibit relatively low temperature dependence of solute permeation and volume fluctuation (96) and as S-layer proteins and many other proteins in Sa-MVs are membrane bound (23). The observed blue shift in emission maximum with increasing temperature may simply arise from (i) thermal agitation that disorders the orientation of solvent dipoles with respect to the excited state dipole moments of protein chromophores and (ii) the thermal-induced increase in distance between solvent dipoles and the excited state dipole moments of protein chromophores, as described by

Macgregor and Weber (97). Unlike the emission maximum, the excitation maximum of dialyzed Sa-MVs does not vary with temperature (Figure 13D), probably due to the low strength of the ground state dipole moment of tryptophans and tyrosines. The steady decrease of the intensity of intrinsic protein fluorescence with increasing temperature (Figure 13C) is expected, as a result of increased dynamic quenching.

Temperature (˚C)	Emission Maximum (nm)
20.0	303.0
24.0	300.0
28.2	298.0
34.7	298.0
47.3	298.0
52.2	295.0
48.0	296.0
34.8	298.0
20.5	303.0

Table 3. **Effect of temperature on the emission maximum of Sa-MV**. Intrinsic fluorescence of Sa-MV in 50 mM pyrophosphate buffer. Excitation wavelength = 275 nm. Red: heating mode; blue: cooling mode. Like the case of Sa-MVs in Tris buffer, a blue shift in $\lambda_{em,max}$ of 8 nm is seen in the intrinsic protein fluorescence when the temperature is changed from 20 to 52.2^{o}C.

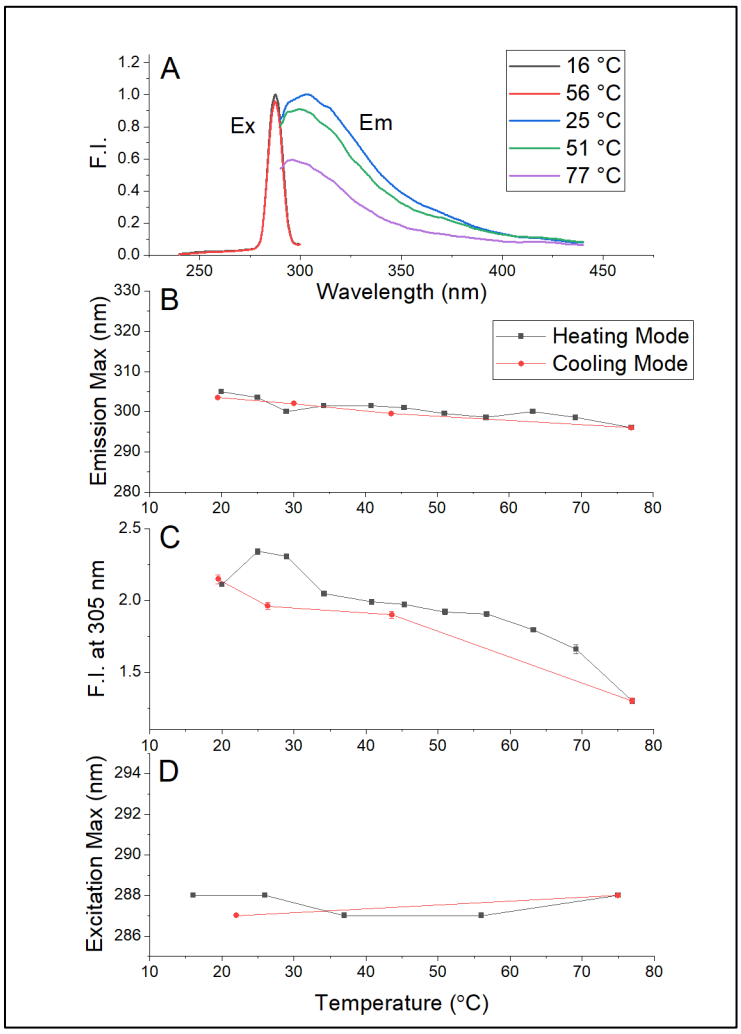

Figure 13. Effect of temperature on the intrinsic protein fluorescence of dialyzed Sa-MVs. (A) illustration of the temperature effect on the emission and excitation spectra; (B-D, respectively) the temperature dependence of the wavelength of the emission maximum ($\lambda_{em,max}$), the fluorescence intensity (F.I.) measured at 305 nm when excited at 275 nm, and the wavelength of the excitation maximum ($\lambda_{ex,max}$).

5.2 Laurdan fluorescence

Laurdan and 6-propionyl-2-dimethylaminonaphthalene (Prodan) have the same chromophore and both probes are extremely sensitive to environmental polarity changes mainly due to changes in solvent relaxation around the probe's excited state (83). In membrane studies, the term "solvent" is referring to the bulk water molecules and the water molecules bound to the lipid polar headgroups as well as the polar residues of the lipids near the probe. Solvent relaxation in the bulk aqueous water is on the picoseconds timescale whereas solvent relaxation due to bound water and nearby lipid polar headgroups occurs in nanoseconds (84), which are more important factors when considering the fluorescence of these probes in membranes.

In proteoliposomes, Prodan, which carries a 3-C propionyl tail, can insert into lipid membranes or bind non-covalently to proteins, whereas Laurdan, which carries a 12-C lauroyl chain, mainly inserts into lipid membranes. Thus, in this study, we chose to use Laurdan as an environmentally sensitive probe to explore the organization and dynamics in the interfacial regions between the lipid hydrophobic core and the lipid polar headgroups in Sa-MV membranes. The results are compared with various LUVs. LUV_{DPPC} and LUV_{POPC} are composed of the diester lipids DPPC and POPC, respectively, whereas lipids in Sa-MVs, LUV_{MV}, and LUV_{PLFE} are exclusively tetraethers as mentioned earlier.

Laurdan can insert into diester lipid membranes with its chromophore located near the polar headgroup regions (85-87) and with its chromophore's dipole moment aligned in parallel with the membrane normal (88). When the membrane packing in diester lipid

membranes is tight and the water content near the chromophore is low, the generalized polarization (GP) value of Laurdan fluorescence is high, and vice versa (89).

Our data on LUV_{DPPC} and LUV_{POPC} shown in Figure 14 are fully consistent with this well-established trend. Below the main phase transition temperature of DPPC (41°C), the GP value is high (0.45 at 20°C); above the transition temperature, GP becomes low (e.g., −0.1 at 50°C) (Figure 14). The abrupt change in GP is centered around 41°C (Figure 14), which reflects the DPPC main phase transition. In the temperature range examined, LUV_{POPC} is entirely in the liquid crystalline state; thus, as expected, there is no abrupt change in GP with temperature and the GP values are low compared to those in LUV_{DPPC} (Figure 14).

The disposition of Laurdan in tetraether lipid membranes is very different from that in diester lipid membranes, as revealed by our previous fluorescence microscopy study on PLFE and DPPC giant unilamellar vesicles (GUVs) (13). The photoselection experiment showed that the dipole moment of Laurdan's chromophore in PLFE GUVs is aligned in parallel with the membrane surface, whereas, in sharp contrast, the dipole moment of Laurdan's chromophore in DPPC GUVs is aligned perpendicular to the membrane surface (13). The most plausible configuration for Laurdan in GUV_{PLFE} is that the lauroyl tail of Laurdan inserts into the hydrocarbon core in parallel with the bidiphytanyl chains while the chromophore resides in the lipid polar headgroup regions with the long molecular axis of the chromophore aligned in parallel with the membrane surface (13). This unusual L-shape disposition for Laurdan in PLFE liposomes is presumably caused by the rigid/tight packing in PLFE liposomes and by the steric hindrance of the branched methyl group in

PLFE lipids (13). In this disposition, the chromophore of Laurdan in GUV_{PLFE} is in close proximity to the bound water molecules at the polar headgroups and close to the lipid headgroup polar moieties (e.g., phosphoinositol and other sugar moieties, Figure 1), and as a result, the degree of "solvent" relaxation is always extensive— hence the low GPs (near zero) at all of the temperatures examined in our previous GUV study (12-66^{o}C) (13). Because the chromophore disposition is different, Laurdan GP values obtained from tetraether lipid membranes cannot be directly compared with those obtained from diester lipid membranes.

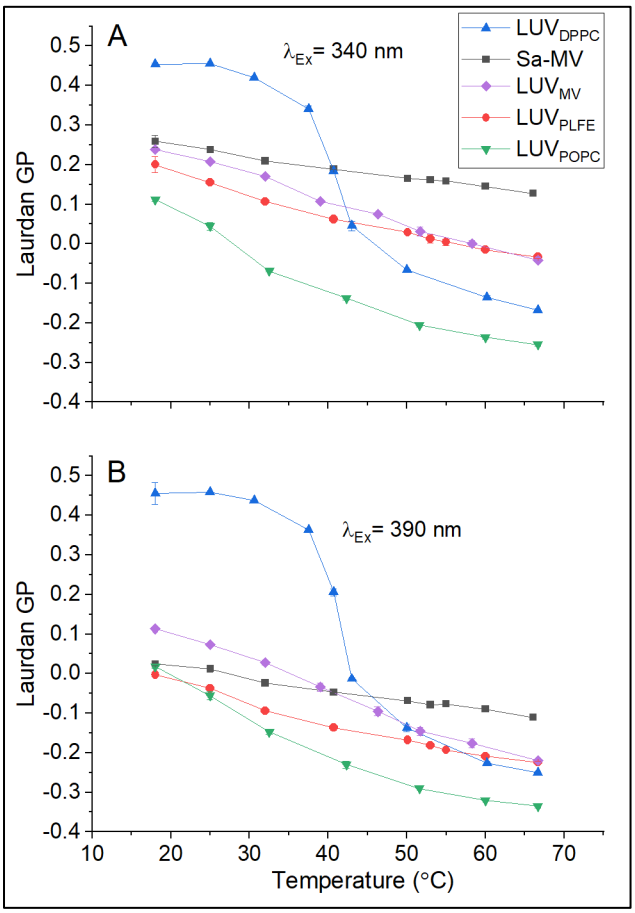

Figure 14. Effects of temperature on Laurdan's excitation generalized polarization (GP) in Sa-MVs and in various liposomes as indicated. (A) λ_{ex} = 340 nm; (B) λ_{ex} = 390 nm. All the samples were in the same Tris buffer described earlier. Error bars are the standard deviations of three measurements.

Figure 14B shows that, when excited at 390 nm, the GP values of LUV_{PLFE} are low (from 0 to −0.2) over the entire temperature range examined (18-68°C), in good agreement with the GP values (from 0 to −0.3 in the temperature range 12-66°C) previously measured from GUV_{PLFE} using the same excitation wavelength (two photon excitation at 780 nm, which is equivalent to one photon excitation at 390 nm) (13). When excited at 340 nm, similar results on the temperature dependence of Laurdan's GP were obtained from LUV_{PLFE} (Figure 14B). In this case, the GP values are slightly higher (Figure 6B) due to the excitation of probe molecules in the less solvent relaxed state. Regardless of the excitation wavelength, the GP values of LUV_{PLFE} are much lower than the GP values of gel state DPPC at any given temperature (Figure 14). It would be totally wrong if these GP data were interpreted as membrane packing in LUV_{DPPC} being tighter than that in LUV_{PLFE} as our previous volume fluctuation measurements clearly showed that membrane packing in PLFE liposomes is much tighter than that in DPPC liposomes (3). Thus, our present data (Figure 14) echo the previous finding that the GP values from tetraether lipid membranes cannot be directly compared with the GP values from diester lipid membranes. This point applies to GUVs as well as LUVs.

It is meaningful to compare Laurdan's GP values in Sa-MVs, LUV_{MV}, and LUV_{PLFE} because lipids in these three membranes are exclusively tetraethers. The compositional differences among these three systems are: (1) Sa-MVs and LUV_{MV}s have GDGT and GTGT as the hydrophobic cores Laurdan's GP whereas LUV_{PLFE}s have GDNT and GDGT as the core structures (Figure 1), (2) polar headgroups in PLFE may be very different from

those in Sa-MV lipids, and (3) Sa-MV membrane is covered by an S-layer and contains membrane-bound proteins whereas LUV_{MV}s and LUV_{PLFE}s are protein free.

In these three systems, Laurdan's GP decreases with increasing temperature monotonically without any abrupt changes. This result implies that there is a continuous reduction in membrane packing tightness as the temperature increases and that there is no sign for lipid phase transitions. This is a piece of new information about Sa-MVs and the LUVs reconstituted from Sa-MV lipids, but a bit puzzling with regards to lipid phase transitions in PLFE liposomes. PLFE GUVs (~10 μm) have previously been shown to exhibit a small phase transition at ~50 ^{o}C by using Laurdan's GP (13). The lack of an abrupt change in GP with temperature in PLFE LUVs (~200 nm) (Figure 14) may be attributed to subtle changes in membrane packing due to the increase in vesicle curvature.

It is also interesting to note that Sa-MVs and LUV_{MV} have higher GP values than LUV_{PLFE}, which suggests that the chromophore experiences less "solvent" relaxation or tighter membrane packing when Laurdan is in Sa-MVs and LUV_{MV}s than in LUV_{PLFE}.

In order to describe membrane packing tightness near the probe's chromophore in a quantitative manner, we have calculated the red edge excitation shift (REES) of Laurdan fluorescence in Sa-MVs and various liposomes. The REES values were calculated by comparing the emission spectra excited at 340 nm (near the excitation maximum) with those excited at 390 nm (the red edge excitation) as described in Materials and Methods.

Figure 15 illustrates how the emission spectrum of Laurdan in these membrane systems changes with the red edge excitation at different temperatures. It is clear from Figure 15 that there is a considerable red shift in the emission spectrum of Laurdan in Sa-MVs,

LUV_{MV}s, and LUV_{PLFE}s when excited at 390 nm. These three membrane systems contain exclusively tetraether lipids. In contrast, a red shift is not immediately obvious for diester liposomes, i.e., LUV_{DPPC} and LUV_{POPC}, by simple visual examination of the emission spectra (Figure 15).

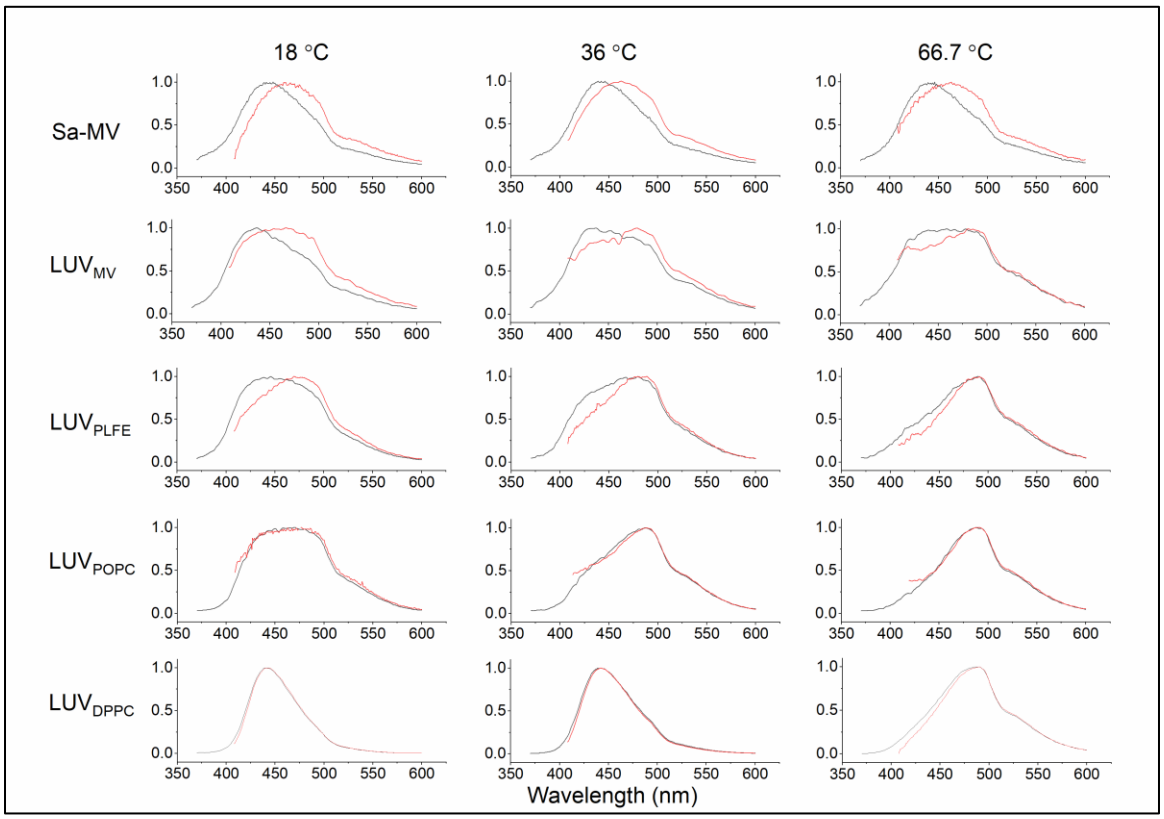

Figure 15. Illustration of technical emission spectra of Laurdan fluorescence in Sa-MVs and various liposomes. Excitation wavelength = 340 nm (black) and red edge excitation wavelength 390 nm (red).

In Figure 16, the calculated REES values are plotted against temperature for all the membrane systems examined (see Table 4). The data indicate that the REES values can be divided into two groups. In the tetraether lipid membrane systems (i.e., Sa-MVs, LUV_{MV}s and LUV_{PLFE}s), the REES values are high (9.3-18.9 nm). In diester lipid membranes (i.e., LUV_{POPC}s and LUV_{DPPC}s), the REES values are relatively low (0.4-5.0 nm). A much higher REES value in tetraether lipid membranes suggests that Laurdan is in a much more motionally restricted environment than Laurdan in diester liposomes at any given temperature examined (90). The high REES and low GP values of Laurdan fluorescence in tetraether lipid membranes suggest that the bound water molecules and the polar lipid moieties in polar headgroup regions of tetraether lipid membranes, where the chromophore of Laurdan resides, are tightly bound among themselves and strongly interact with Laurdan's chromophore. This strong interaction causes the solvent reorientation around the chromophore to occur very slowly in comparison to Laurdan's fluorescence lifetime (91).

Among these three tetraether membrane systems examined, the REES values of Sa-MVs (14.9-18.9 nm) are significantly higher than those in LUV_{MV}s and LUV_{PLFE}s, with a *p* value less than 0.003 comparing Sa-MV to LUV_{PLFE}. It is possible that the crystalline array of the S-layer proteins on top of the tetraether lipid membrane in Sa-MVs provides additional motional restriction of Laurdan. It is also worthy of noting that REES in LUV_{MV}s is higher than that in LUV_{PLFE}s, especially at low temperatures (< 50^{o}C) (Figure 16) and that Sa-MVs and LUV_{MV}s have higher GP values than LUV_{PLFE}s (Figure 14). These data suggest that Laurdan's chromophore experiences tighter membrane packing when Laurdan is in Sa-MVs and LUV_{MV}s than in LUV_{PLFE}s. This packing difference may originate from

the subtle difference in lipid composition. Sa-MV lipids are composed of GDGT (major component) and GTGT whereas PLFE lipids contain GDNT (major component) and GDGT, as mentioned earlier. All three of these lipids are bipolar tetraether macrocyclic or semi-macrocyclic molecules. GDNT has nonitol on one side and glycerol on the other side of the hydrocarbon bore whereas GDGT and GTGT have glycerol at both polar ends. In addition, the polar head-groups on Sa-MV lipids, which are not yet known, may be very different from those seen in PLFE. These differences in chemical structure may lead to changes in hydrogen bonding between Laurdan and lipids and among lipids themselves, all of which can affect membrane packing and solvent reorientation.

Figure 16 shows that there is no abrupt change in REES with temperature in Sa-MVs, LUV_{MV}s, LUV_{PLFE}s, and LUV_{POPC}s, which indicates that there is no major phase transition in those membrane systems in the temperature range examined. These results are consistent with the GP data (Figure 14). In these membranes, the slight decrease in REES with increasing temperature (Figure 16) likely results from the thermal-induced increase in volume fluctuations and consequently a slight increase in the rate of solvent reorientation.

REES in LUV_{DPPC}s undergoes an abrupt change at 41^{o}C (Figure 16), which reflects the main phase transition of DPPC. This result is in excellent agreement with the GP data (Figure 14). However, it is surprising that the REES value is high in DPPC liquid crystalline (fluid) state and low in gel state (Figure 16). Intuitively, this trend would be the other way around. One possible explanation is that REES not only depends on the rate of solvent reorientation around the probe, but also changes with probe location and orientation in the membrane. A recent quantum mechanical and molecular dynamics study (87)

showed that the location and orientation of Laurdan's chromophore in DPPC bilayers have a heterogeneous distribution, rather than a single fixed value, and that the fluorescence properties of Laurdan in lipid bilayers are influenced by the chromophore's orientation and depth of membrane penetration. It is possible that, through the DPPC gel-to-fluid phase transition, the Laurdan's depth penetration and orientation are changed resulting in an increase in REES, despite that solvent reorientation increases with increasing temperature.

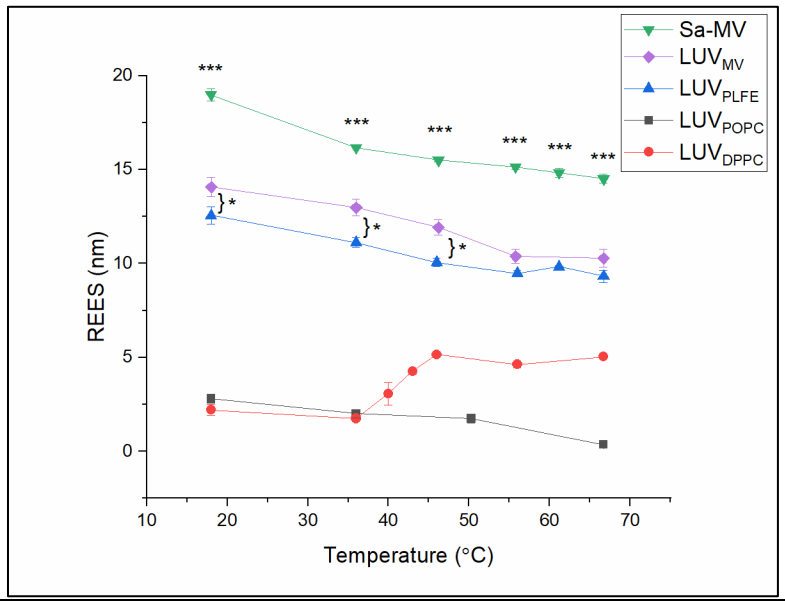

Figure 16. Effect of temperature on REES in Sa-MVs and various liposomes. Error bars are the standard deviations of three measurements. * denotes *p* value < 0.03 comparing LUV_{MV} to LUV_{PLFE} and *** denotes *p* value < 0.003 comparing Sa-MV to LUV_{PLFE}.

Temperature (˚C)	LUV_{POPC}	LUV_{DPPC}	LUV_{PLFE}	Sa-MV	LUV_{MV}
18.0	2.81 ± 0.23	2.21 ± 0.28	12.56 ± 0.47	18.94 ± 0.27	14.03 ± 0.43
36.0	2.01 ± 0.22	1.75 ± 0.14	11.12 ± 0.25	16.18 ± 0.07	12.71 ± 0.44
56.0	--	4.62 ± 0.16	9.48 ± 0.16	15.14 ± 0.14	10.38 ± 0.38
66.7	0.36 ± 0.17	5.04 ± 0.07	9.33 ± 0.33	14.51 ± 0.24	10.16 ± 0.46

Table 4. Sa-MV REES values. The REES values obtained from Sa-MVs and various liposomes at four different temperatures

CHAPTER #6

RESULTS PART 3

6.1 Free Standing Planar Membranes

In Figure 17, we show the ability of two tetraether lipid systems, PLFE and Sa-MV lipid, to form stable free standing planar membranes. Membrane stability was assessed via membrane capacitance, by placing electrodes on either sides of the membrane. When compared to diester lipids POPC and DMPC, it is evident that the tetraether lipid systems can sustain a stable capacitance for a significantly longer period of time. It is very clear that the diester lipid POPC (Figure 17, black curve) is not suitable for planar membrane work, as it was not able to generate stable capacitance readings for longer than 1 hour before capacitance drops to 0 indicating membrane rupture (46). DMPC planar membrane (Figure 17, red curve) was able to hold a constant capacitance for about 2 hours before failing. These results are consistent with previous studies on free standing diester lipid planar membranes (47). Planar membranes made of Sa-MV lipids (blue curve) lasted about 8 hours while PLFE was able to maintain constant capacitance for at least 11 days. The measurement was stopped on Day 11 because the instrument became unavailable at that time. Capacitance values for PLFE were almost entirely unchanged throughout the duration of the experiment (11 days), which indicates that membrane stability was constant.

The difference in this free standing planar membrane stability between MV lipid and PLFE is not presently known. The difference in the hydrophobic core region of these

two systems, as well as the differences in headgroups could be responsible for the difference in stability.

The stability of tetraether lipid systems over diester lipid systems in free standing planar membranes is not a novel finding, (46). The ether linkages and branched chain methyl groups that are present in tetraether lipid membranes lend to much greater stability than the ester linkages and lack of branched chains in diester lipids. This is due to lipid tangling amongst adjacent lipid molecules (52) and the reduction of motion and membrane dynamics within the membrane (53). However, the duration of PLFE planar membrane stability assessed in this study far exceeds the previous study, which lasted several hours as opposed to days. The stability of MV lipid planar membranes has not been assessed at all.

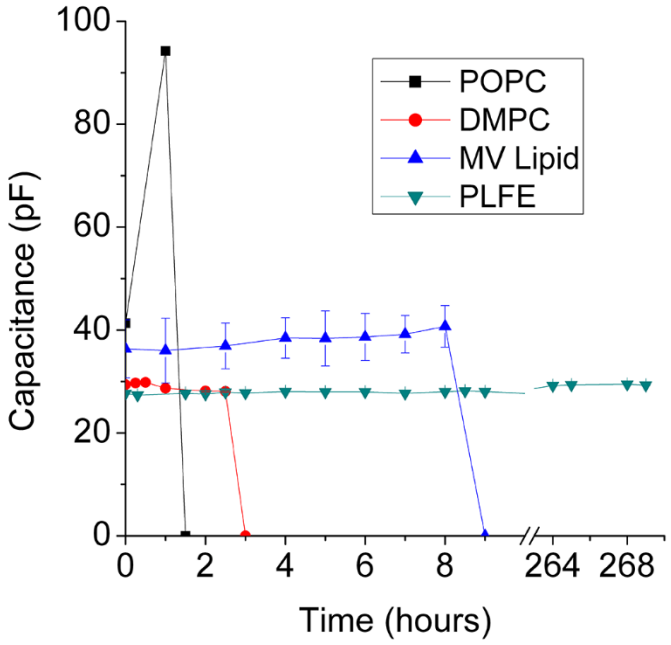

Figure 17. Stability of various free standing planar membranes. Stability was assessed via capacitance of POPC (black) DMPC (red) MV lipid (blue) and PLFE (teal) membranes

6.2 Functional protein incorporation

We have also studied whether membranes made of Sa-MV lipids can accommodate membrane proteins and exhibit protein activities. If they do, Sa-MVs, the reconstituted liposomes and/or planar membranes derived from Sa-MV lipids can be used to develop technological applications. The first part of this section is to test if MTHK channel protein can insert into planar membranes made of Sa-MV lipids and exhibit channel activities. The second part of this section is to test if bacteriorhodopsin (BR) can insert into Sa-MV lipid membranes and exhibit light driven proton pumping activity.

Figure 18 shows channel activity of MTHK in PLFE (A&B) free standing planar membranes, but not in MV lipid free standing planar membranes (C&D). MTHK channels were isolated from the crenarchaeon *Methanothermobacter thermautotrophicus.* This channel was chosen because its native lipid environment with the M. thermautotrophicus membrane also contains tetraether lipids. These lipids are not exactly the same as those comprising PLFE or Sa-MV, but share structural similarities. MTHK activity was monitored by measuring potassium flux through the channel. In PLFE, channel openings and closings were seen at two examined calcium concentrations, 0.1 mM and 1.0 mM calcium. This result shows, for the first time, that MTHK channel can insert into the tightly packed PLFE planar lipid membranes and exhibit channel activities. Another novel finding, is that, at calcium concentrations as low as 0.1 mM, the channel activity of MTHK is still easily detectable. This implies that calcium binding to MTHK is stronger when MTHK is embedded in tetraether lipid membranes, as calcium binding to MTHK is required for channel functionality. In contrast, in diester lipid planar membranes, very little channel

activity is detectable at this low calcium concentration, with open probability of the channel very close to zero in the same pH range (92).

However, no channel activity was observed in planar membranes made of MV lipids under the same conditions. There are a number of reasons why a free standing MV lipid membrane may not be suitable for protein insertion despite it working successfully in PLFE. Firstly, it could be due to the tighter packing of MV lipid membranes, as indicated by higher REES values in LUV_{MV} compared to LUV_{PLFE}. A more tightly packed membrane could make it much more difficult for protein to insert into the membrane. Secondly, the polar head groups on MV lipid molecules could form a much stronger hydrogen bond network than those on PLFE, which make a larger energy barrier for the insertion of membrane proteins. Unfortunately, at present, the polar headgroups on MV lipids have not yet been characterized. Thirdly, the tetraether lipids we extracted from Sa-MVs may contain more cyclpentane rings than PLFE lipids we isolated. Cyclopentane rings can decrease the dynamic motions of hydrocarbon chains in the membrane lipids, thus reducing membrane free volume and volume fluctuations. These effects will hinder membrane protein insertion. It is possible that the number of cyclopentane rings in Sa-MV lipids is higher than that in PLFE lipids, thus MTHK insertion is inhibited. Again, unfortunately, the average number of cyclopentane rings in Sa-MVs is not known.

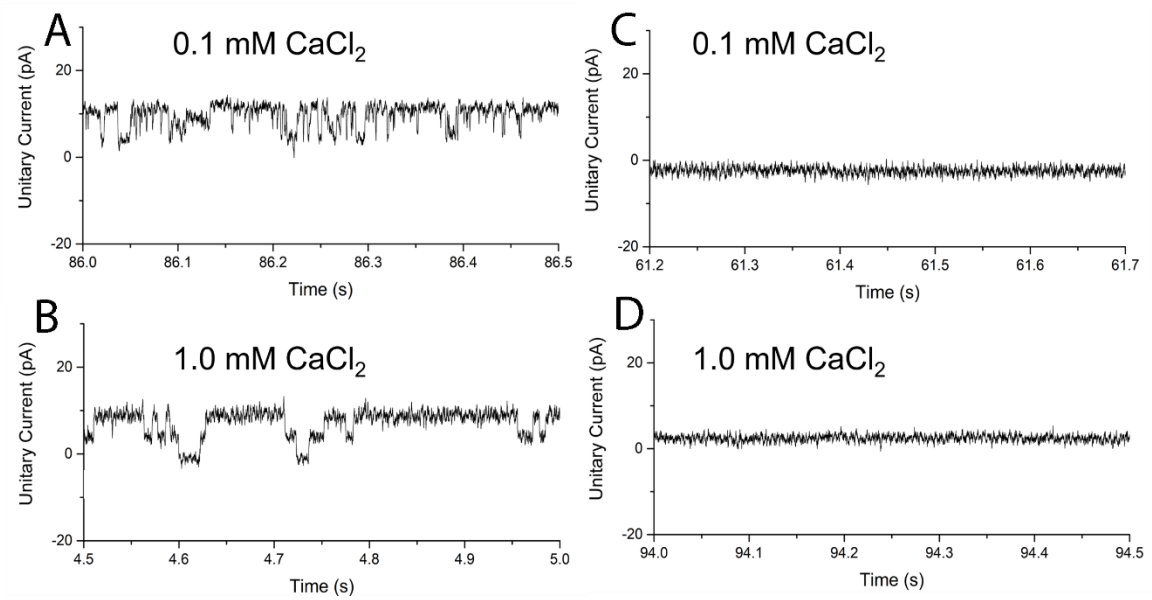

Figure 18. MTHK channel activity in PLFE (A&B) or MV lipid (C&D). Channel activity was recorded at two $CaCl_2$ concentrations as measured by potassium ion flux

Figure 19 shows a fluorescence intensity plot of 5(6)-carboxyfluorescein vs incubation time in response to a pH gradient, excited at 500 nm. Internally, liposomes contained 5mM of 5(6)CF at a near-neutral pH 7.2. A gradient of 4.6 was implied to mimic the external pH of *S. acidocaldarius'* natural environment (2.6). In order to highlight the potential technological applications of tetraether liposomes, bacteriorhodopsin was inserted. Bacteriorhodopsin activates when exposed to green light, and pumps protons from the aqueous environment into the liposome, thereby lowering the pH. The fluorescence intensity of 5(6)CF is pH dependent, decreasing with decreasing pH, and a subsequent response is observed.

In PLFE liposomes (Figure 19), after about 25 minutes of green light exposure, channel activation is observed as the fluorescence intensity drops significantly by 40%. This is compared to PLFE liposomes without bacteriorhodopsin, where a small initial decrease in FI is observed as the liposomes are subjected to low pH, after which FI remains constant throughout the course of the experiment. The low leakage rate of PLFE liposomes that do not contain BR is consistent with the literature (93), as the rigid packing of the lipids within the membrane as well as the branched methyl groups and inositol moiety in the polar head group region allow for very little proton leakage at room temperature. It can be said that the proton flux and subsequent fluorescent intensity decrease in PLFE liposomes containing BR is due entirely to activated BR pumping protons into the liposomal compartment.

Similar to the planar membrane studies, the same effect was not able to be repeated in LUV_{MV}. This is possibly due to the more tightly packed environment of LUV_{MV} than

LUV_{PLFE}, in accordance with the REES data obtained in Figure 16. Higher REES numbers indicate less membrane space, thereby making protein insertion into LUV_{MV} more difficult. In addition, interactions with the polar headgroup regions of MV lipid, which have not yet been identified, will lend different physicochemical properties to LUV_{MV} than LUV_{PLFE}, complicating protein insertion.

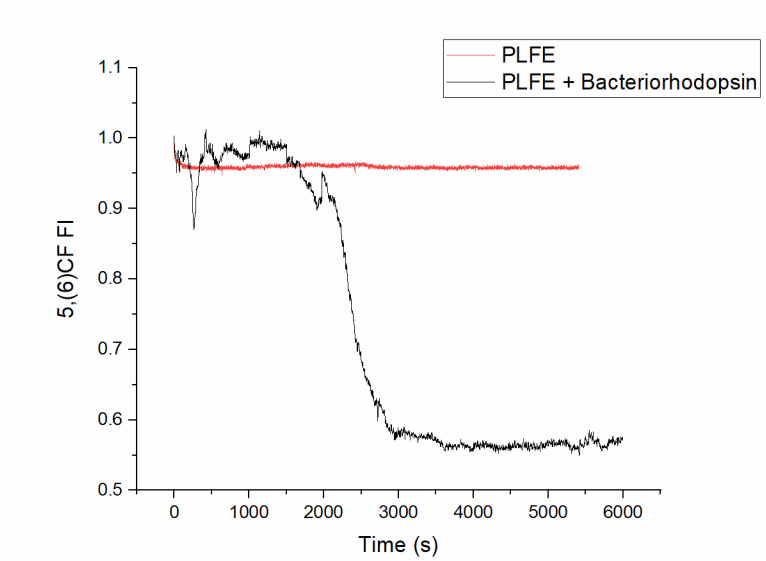

Figure 19. **5, (6)CF intensity change as reflected by pH decrease within liposomes**. CF intensity change within LUV_{PLFE} with (black curve) and without (red curve) bacteriorhodopsin in a 1:400 protein to lipid ratio

CHAPTER # 7

DISCUSSION

Virtually all types of cells can secret microvesicles (MVs). Yet, not all MVs could be useful for technological applications. MVs released from activated platelets, for example, can cause strong pathophysiological effects (94) and are composed of diester lipids, thus not stable against hydrolysis, oxidation, or lipases. In contrast, Sa-MVs are extraordinarily stable because they have lipid membranes made of bipolar tetraethers, which are known to yield tough membranes with strong chemical stability, tight membrane packing and low membrane permeability (32). The S-layer on the surface of Sa-MVs provides an additional protection, allowing only small molecules or peptides with a low molecular weight to go through the pores in the S-layer to enter microvesicles. Compared to MVs released by mammalian and bacterial cells, Sa-MVs are simpler, containing fewer proteins (23). While Sa-MVs are autoclavable as demonstrated in this study, it remains to be demonstrated that native or autoclaved Sa-MVs will not produce any cytotoxicity to healthy cells if they are designed for medical applications.

Sa-MVs, LUV_{MV} and LUV_{PLFE} all contain exclusively tetraether lipids, which are less prone to autoxidation and hydrolysis than diester or diether lipids. The chemical structures of the hydrophobic cores and the polar headgroups of PLFE lipids are well characterized (8) (discussed earlier). When PLFE lipids self-assemble to form vesicular membranes, the polar headgroups form extensive hydrogen bond network at the vesicle surface while the dibiphytanyl chains are rigid and tightly packed in the vesicle's hydrophobic interior (32) so the overall PLFE membrane structure is extremely stable with

little volume fluctuation over a wide temperature range (15-85 ˚C) (67). If the tetraether lipids in Sa-MVs are just like PLFE lipids, then we can easily understand why Sa-MVs are also stable over a wide range of temperatures (Figure 3). At present, the chemical structures of the hydrophobic cores in Sa-MV lipids are known to be GDGT and GTGT, with no GDNT, but the structures in the polar headgroup regions are not known (23). What we know is that, like PLFE, many, if not all, Sa-MV lipids are negatively charged at neutral pH (Figure 6). A sluggish decrease in particle size with surfactant was observed in both Sa-MVs and $LUV_{MV,}$ but not in LUV_{PLFE}, (Figure 9), which may reflect some unique, but unknown, structural properties associated with Sa-MV lipids. The difference between the GDNT (abundant in PLFE, but lacking in Sa-MVs) and GDGT (abundant in Sa-MVs, but little in PLFE) core lies in the calditol moiety versus the glycerol backbone at one polar end of the molecule. Therefore, chemical characterization of Sa-MV lipid polar headgroups is highly needed in order to gain a deeper understanding of the physicochemical properties of Sa-MVs.

Although some man-made liposomes such as those engineered from PLFE are also stable against temperature, pH, and other environmental stressors, Sa-MVs are unique in that they are naturally occurring nanoparticles with a native membrane environment suitable for entrapping small drug molecules and for inserting lipids and membrane-bound proteins as needed. No archaeal pathogens have been reported; therefore, it can be assumed that Sa-MVs released from the thermoacidophilic archaeon *S. acidocaldarius* are not pathogenic either. Based on our present study, it is feasible to use autoclaving to sterilize Sa-MVs and denature nucleic acids and proteins within the microvesicles, while retaining

Sa-MV's stable envelope (membrane plus the S-layer). Further, since various proteins can artificially insert into or move across the Sa-MV membrane and since the S-layer can be easily removed and re-installed (68), it is conceivable that autoclaved Sa-MVs, or MVs released from other crenarchaeota, can be engineered to make stable yet functional nanoparticles or microreactors for a variety of applications such as targeted drug/gene delivery, biocatalysis, biosensing, and vesicular membrane-based artificial photosynthesis.

Intrinsic protein fluorescence/absorption and Laurdan fluorescence together indicate that lipids and proteins in microvesicles of *S. acidocaldarius* (Sa-MVs) is unusually tightly packed over a wide range of temperatures (18-20 to 65-75^{o}C). The emission maximum of Sa-MV intrinsic protein fluorescence at 303 nm is rare, and one of the bluest ever reported, which could result from tight packing in the microvesicles due to, for example, protein J-aggregate formation in the S-layer. Laurdan's GP values in Sa-MVs are low, probably due to the special L-shaped disposition of Laurdan in tetraether lipid membranes in response to tight/rigid membrane packing as previously proposed (13). The REES effect of Laurdan effect is most pronounced in Sa-MVs among all the membranes examined, suggesting "solvent" reorientation around Laurdan's chromophore occurs very slowly due to tight packing. These spectroscopic measurements provide consistent data in support of the proposition that Sa-MVs are unusually tightly packed. This level of understanding may help reveal the structure-activity relationship of Sa-MVs (95) and pave the way for developing Sa-MVs into a useful nanoparticle (Figure 20) (42).

Our data suggest that lipids extracted from *S. acidocaldarius* MVs are able to form fairly stable free-standing planar membranes across a pinhole on a solid support. However,

even though both MV lipids and PLFE lipids are tetraethers, the planar membrane made of MV lipids is not as stable as that made of PLFE lipids. The molecular basis for the differential stability between planar membranes of MV lipids and PLFE lipids is not clearly understood at present, but the difference in stability is likely to originate from the chemical structure differences between PLFE lipids and MV lipids. As mentioned earlier, in terms of the hydrophobic cores, PLFE contains ~90% GDNT and ~10% GDGT, whereas MV lipids are mainly GDGT and GTGT, without any GDNT, and their headgroup structures are not known.

We have also demonstrated the ability to observe channel activity in PLFE monolayers at a range of voltages from -200 to 200 mV. However, this property was not replicated in lipids extracted from *S. acidocaldarius* microvesicles. Since MV lipids can form liposomes, and packing appears to be tighter than PLFE liposomes, LUV_{MV} still hold potential as an incredibly stable nanocarrier. In the future, entrapment of DNA or RNA vectors within these tetraether liposomes leading to expression of target genes in *E. coli* is the next logical step to show functional applications. Similarly, we were able to demonstrate some functionality of bacteriorhodopsin in PLFE liposomes, but not in MV lipid.

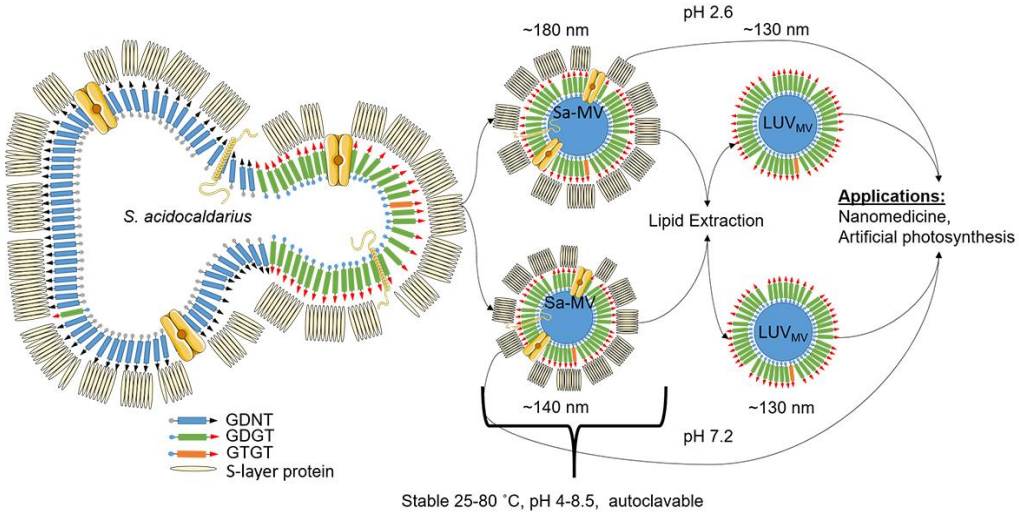

Figure 20. Graphical summary. Illustration rendering Sa-MVs, LUVMV, and their potential applications.

BIBLIOGRAPHY

(1) Woese CR, Kandler O, Wheelis ML. Towards a natural system of organisms: proposal for the domains *Archaea, Bacteria, and Eucarya*. Proc Natl Acad Sci USA 1990;87:4576-4579.

(2) Fliermans CB, Brock TD. Ecology of Sulfur-Oxidizing Bacteria in Hot Acid Soils. Journal of Bacteriology 1972:343-350.

(3) Zhai Y, Chong PL-, Taylor LJ-, Erlkamp M, Grobelny S, Czeslik C, et al. Physical properties of archaeal tetraether lipid membranes as revealed by differential scanning and pressure perturbation calorimetry, molecular acoustics, and neutron reflectometry: effects of pressure and cell growth temperature. Langmuir 2012;28:5211-5217.

(4) Brock TD, Brock KM, Belly RT, Weiss RL. Sulfolobus: a new genus of sulfur-oxidizing bacteria living at low pH and high temperature. Arch Mikrobiol 1972;84:54-68.

(5) Brochier-Armanet C, Boussau B, Gribaldo S, Forterre P. Mesophilic crenarchaeota: proposal for a third archaeal phylum, the Thaumarchaeota. Nature Reviews Microbiology 2008;6:245-252.

(6) Chang EL, Lo S-. Extraction and purification of tetraether lipids from *Sulfolobus acidocaldarius*. Protocols for Archaebacterial Research. Fleischmann, E.M.; Place, A.R.; Robb, R.T.; Schreier, H.J. ed. Baltimore, MD: Maryland Biotechnology Institute; 1991. p. 2.3.1-2.3.14.

(7) Lo SL, Montague CE, Chang EL. Purification of glycerol dialkyl nonitol tetraether from *Sulfolobus acidocaldarius*. J Lipid Res 1989 Jun;30(6):944-949. 87

(8) Lo SL, Chang EL. Purification and characterization of a liposomal-forming tetraether lipid fraction. Biochem Biophys Res Commun 1990 Feb 28;167(1):238-243.

(9) Chong PL-, Ayesa U, Daswani VP, Hur EC. On physical properties of tetraether lipid membranes: Effects of cyclopentane rings. Archaea 2012;2012:Article ID 138439.

(10) De Rosa M, Esposito E, Gambacorta A, Nicholaus B, Bu'lock JD. Effects of temperature on ether lipid composition of *Caldariella acidophila*. Phytochemistry 1980;19:827-831.

(11) Chong, P. L. -G., Bonanno, A.P., Ayesa, U. **Dynamics and Organization of Archaeal Tetraether Lipid Membranes**. In: Chattopadhyay A, editor. Membrane Organization and Dynamics. 20th ed. Springer, Cham: Springer Series in Biophysics; 2019. p. 11-30.

(12) De Rosa M, Gambacorta A, Nicolaus B, Chappe B, Albrecht P. Isoprenoid ethers: backbone of complex lipids of the archaebacterium *Sulfolobus solfataricus*. Biochim Biophys Acta 1983;753:249-256.

(13) Bagatolli LA, Gratton E, Khan TK, Chong PL-. Two-photon fluorescence microscopy studies of bipolar tetraether giant liposomes from thermoacidophilic archaebacteria *Sulfolobus acidocaldarius*. Biophys J 2000 Jul;79(1):416-425.

(14) Chong PL-, Ravindra R, Khurana M, English V, Winter R. Pressure perturbation and differential scanning calorimetric studies of bipolar tetraether liposomes derived from the thermoacidophilic archaeon *Sulfolobus acidocaldarius*. Biophys J 2005;89:1841-1849. 88

(15) Daswani VP. Fluorescence and aggregation properties of the anti-cancer drug CA4P in archaeal liposomes. 2015.

(16) Raposo G, Stoorvogel W. Extracellular vesicles: Exosomes, microvesicles, and friends. The Journal of cell biology 2013;200:373-383.

(17) Deatherage BL, Cooksona BT. Membrane vesicle release in bacteria, eukaryotes, and archaea: a conserved yet underappreciated aspect of microbial life. Infection and Immunity (2012) 80, 1948-1957 2012;80:1948-1957.

(18) Prangishvili D, Holz I, Stieger E, Nickell S, Kristjansson JK, Zillig W. Sulfolobicins, specific proteinaceous toxins produced by strains of the extremely thermophilic archaeal genus *Sulfolobus*. J Bacteriol 2000;182:2985-2988.

(19) Wolf P. The nature and significance of platelet products in human plasma. Br J Haematol 1967;13:269-288.

(20) Ratajczak J, Wysoczynski M, Hayek F, Janowska-Wieczorek A, and Ratajczak MZ. Membrane-derived microvesicles: important and underappreciated mediators of cell-to-cell communication. Leukemia 2006;20:1487-1495.

(21) Gill S, Catchpole R, Forterre P. Extracellular membrane vesicles in the three domains of life and beyond. FEMS Microbiol Rev 2018;43:273-302.

(22) Tozer GM, Prise VE, Wilson J, Locke RJ, Vojnovic B, Stratford MR, et al. Combretastatin A-4 phosphate as a tumor vascular-targeting agent: early effects in tumors and normal tissues. Cancer Res 1999 Apr 1;59(7):1626-1634. 89

(23) Ellen AF, Albers SV, Huibers W, Pitcher A, Hobel CF, Schwarz H, et al. Proteomic analysis of secreted membrane vesicles of archaeal *Sulfolobus* species reveals the presence of endosome sorting complex components. Extremophiles 2009;13:67-79.

(24) Conde-Vancelles J, Rodriguez-Suarez E, Embade N, Gil D, Matthiesen R, Valle M, et al. Characterization and comprehensive proteome profiling of exosomes secreted by hepatocytes. J Proteome Res 2008;7:5157-5166.

(25) Pisitkun T, Shen R-, Knepper MA. Identification and proteomic profiling of exosomes in human urine. PNAS 2004;101:13368-13373.

(26) Gaudin M, Gauliard E, Schouten S, Houel-Renault L, Lenormand P, Marguet E, et al. Hyperthermophilic archaea produce membrane vesicles that can transfer DNA. Environmental Microbiology Reports 2013;5:109-116.

(27) Pohlschroder M, Pfeiffer F, Schulze S, Halim MFA. Archaeal cell surface biogenesis. FEMS Microbiol Rev 2018;42:694-717.

(28) Rodrigues-Oliveira T, Belmok A, Vasconcellos D, Schuster B, Kyaw CM. Archaeal S-layers: overview and current state of the art. Frontiers in Microbiology 2017;8:2597-doi:10.3389/fmicb.2017.02597.

(29) Sa'ra M, Sleytr UB. S-layer proteins. J Bacteriology 2000;182:859-868.

(30) Pum D, Toca-Herrera JL, Sleytr UB. S-layer protein self-assembly. Int J Mol Sci 2013;14:2484-2501.

(31) Gliozzi A, Relini A, Chong PL-G. Structure and permeability properties of biomimetic membranes of bolaform archaeal tetraether lipids. J Membr Sci 2002;206:131-147. 90

(32) Chong PL-. Archaebacterial bipolar tetraether lipids: physico-chemical and membrane properties. Chem Phys Lipids 2010;163:253-265.

(33) Sprott GD, Patel GB, Krishnan L. Archaeobacterial ether lipid liposomes as vaccine adjuvants. Methods Enzymol 2003;373:155-172.

(34) Rethore G, Montier T, Le Gall T, Delepine P, Cammas-Marion S, Lemiegre L, et al. Archaeosomes based on synthetic tetraether-like lipids as novel versatile gene delivery systems. Chem Commun (Camb) 2007 May 28;(20)(20):2054-2056.

(35) Parmentier J, Hofhaus G, Thomas S, Cuesta LC, Gropp F, Schroder R, et al. Improved oral bioavailability of human growth hormone by a combination of liposomes containing bio-enhancers and tetraether lipids and omeprazole. Journal of Pharmaceutical Sciences 2014;103:3985-3993.

(36) Patel GB, Sprott GD. Archaeobacterial ether lipid liposomes (archaeosomes) as novel vaccine and drug delivery systems. Crit Rev Biotechnol 1999;19(4):317-357.

(37) Gonzalez-Paredes A, Clares-Naveros B, Ruiz-Martinez MA, Durban-Fornieles JJ, Ramos-Cormenzana A, Monteoliva-Sanchez M. Delivery systems for natural antioxidant compounds: Archaeosomes and archaeosomal hydrogels characterization and release study. Int J Pharm 2011 Dec 15;421(2):321-331.

(38) Daswani VP, Ayesa U, Venegas B, Chong PL-. Concentration-induced J-aggregate formation causes a biphasic change in the release of *trans*-combretastatin A4 disodium phosphate from archaeosomes and the subsequent cytotoxicity on mammary cancer cells. Molecular Pharmaceutics 2015;12:3724-3734. 91

(39) Uhl P, Pantze S, Storck P, Parmentier J, Witzigmann D, Hofhaus G, et al. Oral delivery of vancomycin by tetraether lipid liposomes. European Journal of Pharmaceutical Sciences 2017;108:111-118.

(40) Pichler H, Emmersturfer-Augustin A. Modification of membrane lipid compositions in single-celled organisms - from basic to applications. Method 2018;147:50-65.

(41) Ren X, Kumbur EC, Zhou JG, Noh HM, Chong PL-. Stability of free-standing tetraether planar membranes in microchips. J Membrane Science 2017;540:27-34.

(42) Bonanno A, Chen K, Chong PL-. *Sulfolobus acidocaldarius* microvesicles are naturally occurring nanoparticles with unusual stability against various environmental stressors. Materialia 2019;7:100405.

(43) de Jong J, Lammertink RGH, Wessling M. Membranes and microfluidics: a review. Lab Chip 2006;6:1125-1139.

(44) van den Hurk R, Evoy S. A review of membrane-based biosensors for pathogen detection. Sensors 2015;15:14045-14078.

(45) Choi H-, Montemagno CD. Biosynthesis within a bubble architecture. Nanotechnology 2006;17:2198-2202.

(46) Ren X, Kumber EC, Zhou JG, Noh M, Chong PL-. Stability of free-standing tetraether planar membranes in microchips. J Membr Sci 2017;540:27-34.

(47) Schmidt C, Mayer M, Vogel H. A chip-based biosensor for the functional analysis of single ion channels. Angew Chem Int 2000;39:3137-3140. 92

(48) Han X, Studer A, Sehr H, Geissbuhler I, Di Berardino M, Winkler FK, et al. Nanopore arrays for stable and functional free-standing lipid bilayers. Advanced Materials 2007;19:4466-4470.

(49) Meier W, Nardin C, Winterhalter M. Reconstitution of channel proteins in (polymerized) ABA triblock copolymer membranes. Angew Chem Int Ed 2000;39:4599-4602.

(50) Ren X, Liu K, Zhang Q, Noh HM, Kumbur EC, Yuan WW, et al. Design, fabrication and characterization of archaeal tetraether free-standing planar membranes in a PDMS- and PCB-based fluidic platform. ACS Applied Materials & Interfaces 2014;6:12618-12628.

(51) Elferink MG, de Wit JG, Demel R, Driessen AJ, Konings WN. Functional reconstitution of membrane proteins in monolayer liposomes from bipolar lipids of *Sulfolobus acidocaldarius*. J Biol Chem 1992 Jan 15;267(2):1375-1381.

(52) Shinoda W, Mikami M, Baba T, Hato M. Molecular dynamics study on the effect of chain branching on the physical properties of lipid bilayers: structural stability. J Phys Chem B 2003;107:14030-14035.

(53) Shinoda W, Mikami M, Baba T, Hato M. Dynamics of a highly branched lipid bilayer: a molecular dynamics study. Chem Phys Lett 2004;390:35-40.

(54) Shinoda W, Mikami M, Baba T, Hato M. Molecular dynamics study on the effects of chain branching on the physical properties of lipid bilayers: 2. permeability. J Phys Chem 2004;108:9346-9356. 93

(55) Zadek B, Nimigean CM. Calcium-dependent Gating of MthK, a Prokaryotic Potassium Channel. Journal of General Physiology 2006;6:673-685.

(56) Zeikus JG, Wolfe RS. Fine Structure of Methanobacterium thermoautotrophicum: Effect of Growth Temperature on Morphology and Ultrastructure. Journal of Bacteriology 1973;113:461-467.

(57) Pitard B, Richard P, Dunach M, Girault G, Rigaud J-. ATP synthesis by the FoF1 ATP synthase from thermophilic Bacillus PS3 reconstituted into liposomes with bacteriorhodopsin. Eur J Biochem 1996;235:769-778.

(58) Wagner N, Gutweiler M, Pabst R, Dose K. Coreconstitution of bacterial ATP synthase with monomeric bacteriohodopsin into liposomes. Eur J Biochem 1987;165:177-183.

(59) Bartlett GR. Phosphorus assay in column chromatography. J Biol Chem 1959 Mar;234(3):466-468.

(60) Blake RCI, Griff MN. In situ spectroscopy on intact Leptospirillum ferrooxidants reveals that reduced cytochrome 579 is an obligatory intermediate in the aerobic iron respiratory chain. Front Microbiol 2016;7:1963.

(61) Rothbauer M, Kupcu S, Sticker D, Sleytr UB, Ertl P. Exploitation of S-layer anisotropy: pH-dependent nanolayer orientation for cellular micropatterning. ACS Nano 2013;7:8020-8030.

(62) Gabriel JL, Chong PL-G. Molecular modeling of archaebacterial bipolar tetraether lipid membranes. Chem Phys Lipids 2000 Apr;105(2):193-200. 94 (63) Kanichay R, Boni LT, Cooke PH, Khan TK, Chong PL-G. Calcium-induced aggregation of archaeal bipolar tetraether liposomes derived from thermoacidophilic archaeon *Sulfolobus acidocaldarius*. Archaea 2003;1:175-183.

(64) Zuidam NJ, Talsma H, Crommelin DJA. Sterilization of liposomes. In: Barenholz Y, Lasic DD, editors. Handbook of Nonmedical Applications of Liposomes, Vol. III: From Design to Microreactors Boca Raton, Florida: CRC press; 2018.

(65) Brown DA, Venegas B, Cooke PH, English V, Chong PL-. Bipolar tetraether archaeosomes exhibit unusual stability against autoclaving as studied by dynamic light scattering and electron microscopy. Chem Phys Lipids 2009;159:95-103.

(66) Helenius A, Simons K. Solubilization of membranes by detergents. Biochim Biophys Acta 1975;415:29-79.

(67) Zhai Y, Chong PL-, Taylor LJ-, Erlkamp M, Grobelny S, Czeslik C, et al. Physical properties of archaeal tetraether lipid membranes as revealed by differential scanning and pressure perturbation calorimetry, molecular acoustics, and neutron reflectometry: effects of pressure and cell growth temperature. Langmuir 2012;28:5211-5217.

(68) Sleytr UB, Schuster B, Egelseer E-, Pum D. S-layers: principles and applications . FEMS Microbiol Rev 2014;38:823-864.

(69) Jameson DM. Introduction to Fluorescence. Boca Raton, FL: CRC Press; 2014. 95

(70) Buddanavar AT, Nandibewoor ST. Multi-spectroscopic characterization of bovine serum albumin upon interaction with atomoxetine. J of Pharmaceutical Analysis 2017;7:148-155.

(71) Jameson DM, Gratton E, Eccleston JF. Intrinsic fluorescence of elongation factor Tu in its complexes with GDP and elongation factor Ts. Biochemistry 1987;26:3894-3901.

(72) Peyfoon E, Meyer B, Hitchen PG, Panico M, Morris HR, Haslam SM, et al. The S-layer glycoprotein of the crenarchaeote *Sulfolobus acidocaldarius* is glycosylated at multiple sites with chitobiose-linked N-glycans. Archaea 2010;2010:754101.

(73) Veith A, Kling A, Zolghadr B, Lauber K, Mentele R, Lottspeich F, et al. *Acidianus, Sulfolobus and Metallosphaera* surface layers: structure, composition and gene expression. Molecular Microbiology 2009;73:58-72.

(74) Teale FWJ, Weber G. Ultraviolet fluorescence of the aromatic amino acids. Biochem J 1957;65:476-482.

(75) Finazzi-Agro A, Rotilio G, Avigliano L, Guerrieri P, Boffi V, Mondovi B. Environment of copper in Pseudomonas fluorescens azurin: fluorometric approaches. Biochemistry 1970;9:2009-2014.

(76) Gilardi G, Mei G, Rosato N, Canters GW, Finazzi-Agro A. Unique environment of Trp48 in *Pseudomonas aeruginosa* azurin as probed by site-directed mutagenesis and dynamic fluorescence spectroscopy. Biochemistry 1994;33:1425-1432.

(77) Soderlind E, Karlsson L. Haemolytic activity of maltopyranoside surfactants. European J Pharm Biopharm 2006;62:254-259. 96

(78) Heerklotz H. Interactions of Surfactants with Lipid Membranes. Quarterly reviews of biophysics 2008;41:205-264.

(79) Lichtenberg D, Ahyayauch H, Goni FM. The mechanism of detergent solubilization of lipid bilayers. Biophys J 2013;105:289-299.

(80) Shapiro BI. Molecular assemblies of polymethine dyes. Russian Chemical Reviews 2006;75:433-456.

(81) Kaiser TE, Scheblykin IG, Thomsson D, Wurthner F. Temperature-dependent exciton dynamics in J-aggregates--When disorder plays a role. J Phys Chem B 2009;113:15836-15842.

(82) Scheblykin IG, Bataiev MM, Van der Auweraer M, Vitukhnovsky AG. Dimensionality and temperature dependence of the radiative lifetime of J-aggregates with Davydov splitting of the exciton band. Chem Phys Lett 2000;316:37-44.

(83) Weber G, Farris FJ. Synthesis and spectral properties of a hydrophobic fluorescent probe: 6-propionyl-2-(dimethylamino)naphthalene. Biochemistry 1979 Jul 10;18(14):3075-3078.

(84) Barucha-Kraszewska J, Kraszewski S, Jurkiewicz P, Ramseyer C, Hof M. Numerical studies of the membrane fluorescent dyes dynamics in ground and excited states. Biochim Biophys Acta 2010;1798:1724-1734.

(85) Chong PL-G. Interactions of Laurdan with Membranes at High Pressures. High Pressure Research 1990;5:761-763. 97

(86) Jurkiewicz P, Olzynska A, Langner M, Hof M. Headgroup hydration and mobility of DOTAP/DOPC bilayers: a fluorescence solvent relaxation study. Langmuir 2006;22:8741-8749.

(87) Baig MW, Pederzoli M, Jurkiewicz P, Cwiklik L, Pittner J. Orientation of Laurdan in phospholipid bilayers influences its fluorescence: quantum mechanics and classical molecular dynamics study. Molecules 2018;23:1707.

(88) Bagatolli LA. LAURDAN fluorescence properties in membranes: a journey from the fluorometer to the microscope. In: Mely Y, Duportail G, series editor Hof M, editors. Fluorescent Methods to study Biological Membranes. Springer Series on Fluorescence 13 ed. NY, NY: Springer; 2013. p. 3-36.

(89) Parasassi T, De Stasio G, Ravagnan G, Rusch RM, Gratton E. Quantitation of lipid phases in phospholipid vesicles by the generalized polarization of Laurdan fluorescence. Biophys J 1991 Jul;60(1):179-189.

(90) Demchenko AP. The red-edge effects: 30 years of exploration. Luminescence 2002;17:19-42.

(91) Mukherjee S, Chattopadhyay A. Wavelength-selective fluorescence as a novel tool to study organization and dynamics in complex biological systems. J of Fluorescence 1995;5:237-246.

(92) Pau VPT, Abarca-Heidemann K, Rothberg B. Allosteric mechanism of Ca2+ activation and H+-inhibited gating of the MthK K+ channel. J Gen Physiol 2010;135:509-526. 98

(93) Komatsu H, Chong PL-. Low permeability of liposomal membranes composed of bipolar tetraether lipids from thermoacidophilic archaebacterium *Sulfolobus acidocaldarius*. Biochemistry 1998 Jan 6;37(1):107-115.

(94) Badimon L, Suades R, Fuentes E, Palomo I, Padró T. *Role of platelet-derived microvesicles as crosstalk mediators in atherothrombosis and future pharmacology targets: A link between inflammation, atherosclerosis, and thrombosis*. Front Pharmacol 2016;7:293-doi: 10.3389/fphar.2016.00293.

(95) Gill S, Catchpole R, Forterre P. Extracellular membrane vesicles in the three domains of life and beyond. FEMS Microbiol Rev 2019;43:273-303.

(96) Weber G, Farris FJ. Synthesis and spectral properties of a hydrophobic fluorescent probe: 6-propionyl-2-(dimethylamino)naphthalene. Biochemistry 1979 Jul 10;18(14):3075-3078

(97) Macgregor RB, Weber G. Estimation of the polarity of the protein interior by optical spectroscopy. Nature 1986;319:70-73.